



1 **Influence of low-frequency variability on high and low groundwater** 2 **levels: example of aquifers in the Paris Basin**

3 Lisa Baulon^{1,2}, Nicolas Massei¹, Delphine Allier², Matthieu Fournier¹, H el ene Bessiere²

4 ¹Normandie Univ, UNIROUEN, UNICAEAN, CNRS, M2C, 76000 Rouen, France

5 ²BRGM, 3 av. C. Guillemin, 45060 Orleans Cedex 02, France

6 *Correspondence to:* Lisa Baulon (lisa.baulon@etu.univ-rouen.fr)

7 **Abstract.** Groundwater levels (GWL) very often fluctuate over a wide range of timescales (infra-annual, annual, multi-
8 annual, decadal). In many instances, aquifers act as low-pass filters, dampening the high-frequency variability and
9 amplifying low-frequency variations (from multi-annual to decadal timescales) which basically originate from large-scale
10 climate variability. In the aim of better understanding and ultimately anticipating groundwater droughts and floods, it
11 appears crucial to evaluate whether (and how much) the very high or very low GWLs are sensitive to such low-frequency
12 variability (LFV), which was the main objective of the study presented here. As an example, we focused on exceedance and
13 non-exceedance of the 80% and 20% GWL percentiles respectively, in the Paris Basin aquifers over the 1976-2019 period.
14 GWL time series were extracted from a database consisting of relatively undisturbed GWL time series regarding
15 anthropogenic influence (water abstraction by either continuous or periodic pumping) over Metropolitan France. Based on
16 this dataset, our approach consisted of exploring the effect of GWL low-frequency components on threshold exceedance and
17 non-exceedance by successively filtering out low-frequency components of GWL signals using maximum overlap discrete
18 wavelet transform (MODWT). Multi-annual (~7-yr) and decadal (~17-yr) variabilities were found to be the predominant
19 LFVs in GWL signals, in accordance with previous studies in the northern France area. Filtering out these components
20 (either independently or jointly) to (i) examine the proportion of high level (HL) and low level (LL) occurrences generated



21 by these variabilities, (ii) estimate the contribution of each of these variabilities in explaining the occurrence of major
22 historical events associated to well-recognized societal impacts.

23 A typology of GWL variations in Paris Basin aquifers was first determined by quantifying the variance distribution across
24 timescales. Four GWL variation types could be found according to the predominance of annual, multi-annual or/and decadal
25 variabilities in these signals: decadal dominant (type iD), multi-annual and decadal dominant (type iMD), annual dominant
26 (type cA), annual and multi-annual dominant (type cAM). We observed a clear dependence of high and low GWL to LFV
27 for aquifers exhibiting these four GWL variation types. In addition, the respective contribution of multi-annual and decadal
28 variabilities in the threshold exceedance varied according to the event. In numerous aquifers, it also appeared that the
29 sensitivity to LFV was higher for LL than HL. A similar analysis was conducted on the only available long-term GWL time
30 series which covered a hundred years. This allowed us to highlight a potential influence of multidecadal variability on HL
31 and LL too.

32 This study underlined the key role of LFV in the occurrence of HL and LL. Since LFV originates from large-scale stochastic
33 climate variability as demonstrated in many previous studies in the Paris Basin or nearby regions, our results point out that i)
34 poor representation of LFV in General Circulation Models (GCM) outputs used afterwards for developing hydrological
35 projections can result in strong uncertainty in the assessment of future groundwater extremes (GWE), ii) potential changes in
36 the amplitude of LFV, be they natural or induced by global climate change, may lead to substantial changes in the
37 occurrence and severity of GWE for the next decades. Finally, this study also stresses the fact that due to the stochastic
38 nature of LFV, no deterministic prediction of future GWE for the mid- or long term horizons can be achieved even though
39 LFV may look periodic.

40 **1. Introduction**

41 The knowledge of hydroclimatic extremes is a major concern in a global change context. Hydroclimatic extremes, leading to
42 droughts or floods, can have major consequences on our societies. During hydrological drought periods, many restrictions of
43 water uses can be imposed to the population. For instance each summer in France, regular restrictions are imposed due to
44 hydrogeological droughts (Maréchal and Rouillard, 2020). These restrictions are damaging especially for agricultural and



45 industrial activities. Floods are equally harmful, the best-known example across France is the flooding of the Somme River
46 Basin in 2001. This flooding cost 100 million euros of damages and 1100 people were evacuated due to the event long
47 duration spreading over several months (Deneux and Martin, 2001). Moreover, flooding events can also lead to other
48 damages such as erosive events or the degradation of water quality.

49

50 The hydrological droughts are characterised by below-normal groundwater levels (GWL) or water levels in lakes, declining
51 wetland area and decreased streamflow (Van Loon, 2015). Surface and subsurface water resources are then inadequate for
52 established water uses of a given water resources management system (Mishra and Singh, 2010). Many studies about
53 hydrological droughts focus on streamflow, but it is equally important to look at aquifers and GWL. Consequently, Mishra
54 and Singh (2010) introduced groundwater drought as a new type of drought alongside the four main types of droughts:
55 meteorological drought, hydrological drought, agricultural drought, socioeconomic drought. Groundwater droughts occur on
56 time scales from months to years (Van Lanen and Peters, 2000). They follow periods of precipitation deficits combined with
57 high evapotranspiration rates, that in turn causes low soil moisture content and low groundwater recharge. Abstraction of
58 groundwater can also enhance naturally occurring droughts (Van Lanen and Peters, 2000). Groundwater droughts may also
59 have consequences on streamflow with less support of the water table during low river flow periods. This can be highly
60 problematic especially in catchments where rivers are strongly sustained by water tables, such as the Seine river where 81%
61 of the flow is supported by groundwater (Flipo et al., 2020).

62

63 Contrastingly to hydrological droughts, that are processes setting up slowly, floods are fast phenomena resulting from
64 extreme precipitation, snowmelt and high initial soil moisture (Berghuijs et al., 2016; Wasko and Nathan, 2019; Bertola et
65 al., 2021). In case of GWL, the speed of emergence of extremely high levels can vary greatly according aquifers and the
66 GWL variation type. In reactive systems, the water table quickly reacts to an exceptional rainy winter leading to high GWL
67 at the end of the recharge period. In inertial systems, several years of exceptional rainfall and recharge are needed to reach
68 particularly high levels. In both cases, extremely high GWL can lead to groundwater flooding. A key example in France was
69 the 2001 floodings in the Somme region that were the consequence of exceptional GWL (higher than the soil surface) and



70 exceptional levels of Somme river. These floodings were the result of above-average winter rainfall during several years
71 rising GWL in the chalk – with limited summer recession of GWL – and an exceptional previous winter with strong
72 precipitation leading to rapidly increase levels of 10m generating the disastrous floodings (Deneux and Martin, 2001; Habets
73 et al., 2010). This 2001 event arised from both a low-frequency variability (LFV) with a slow increase of GWL during
74 several years and a high-frequency variability that is superimposed, with a sudden rise of GWL during the 2000-2001 winter
75 (Pointet et al., 2003).

76

77 It is expected with the climate change to observe increasingly hydroclimatic extremes with stronger intensities and/or higher
78 frequencies (IPCC, 2012; Hirabayashi et al., 2013; Trambly et al., 2020). Therefore in the litterature, studies on
79 hydroclimatic extremes deal very often with trend analyses to identify potential increases in the frequency of extremes and
80 their intensity (Hodgkins et al., 2017; Mangini et al., 2018; Blösch et al., 2019; Vicente-Serrano et al., 2021). To describe the
81 long-term evolution of hydroclimatic extremes and their characteristics (e.g., duration, magnitude, intensity), meteorological
82 or hydrological drought indices such as the Standardised Precipitation Index (SPI; McKee et al., 1993), Standardised
83 Precipitation Evapotranspiration Index (SPEI; Vicente-Serrano et al., 2010), Standardised Streamflow Index (SSI; Vicente-
84 Serrano et al., 2012), Standardised Groundwater level Index (SGI; Bloomfield and Marchant, 2013), are commonly used.
85 These indices are widely used to detect trends in meteorological or hydrological droughts and their variability across time
86 (Vicente-Serrano et al., 2021). However, although these indices are useful tools to describe droughts, their principal limit
87 arises from the standardisation allowing for spatial comparison but therefore hindering to keep the variance notion in time
88 series. For instance, this can be particularly limiting to understand the emergence of high and low GWL whose amplitude
89 seems highly dependent of the maximum water level fluctuation.

90

91 In addition, the long-term effects of climate change on meteorological and hydrological variables may be modified by the
92 internal climate variability leading to their amplification, attenuation, or inversion (Fatichi et al., 2014; Gu et al., 2019).
93 Therefore, it is crucial to better understand the large-scale origin of these LFV variabilities and how catchments can filter
94 and modify them, in particular for prediction purposes. In this regard, Gudmundsson et al. (2011) indicated that the LFV of



95 runoff directly originates from the large-scale atmospheric circulation, while the catchments properties control the proportion
96 of variance of LFV in hydrological variables. Simultaneously, a large amount of studies addressed the large-scale origins of
97 such variabilities in hydroclimatic variables (streamflow, precipitation, groundwater, temperature), using climate indices and
98 atmospheric fields (Massei et al., 2010; Boé and Habets, 2014; Dieppois et al., 2013; Dieppois et al., 2016; Massei et al.,
99 2017; Neves et al., 2019; Liesch and Wunsch, 2019).

100

101 In northern France, more particularly in the Seine watershed, many studies highlighted ~7-yr and ~17-yr variabilities in
102 precipitation and streamflow (Massei et al., 2007; Massei et al., 2010; Fritier et al., 2012; Massei and Fournier, 2012;
103 Dieppois et al., 2013; Massei et al., 2017). Since then, CaWaQS model calibration – that is a Seine Basin Model – is
104 achieved on 17-year period as it is proved that groundwater and river water storage are stationary over such period (Flipo et
105 al., 2012; Flipo et al., 2020). The North Atlantic Oscillation (NAO) was described as one significant driver of such temporal
106 signature (~7-yr and ~17-yr) in precipitation and streamflow (Massei et al., 2007; Massei et al., 2010). Later, Massei et al.
107 (2017) highlighted using a composite analysis with Sea Level Pressure (SLP) that the atmospheric pattern associated to the
108 ~7-yr variability was not exactly reminiscent of the NAO, with centers of action actually shifted to the North. Similarly, the
109 pattern associated to ~17-yr variability (called “~19.3-yr component” in Massei et al. (2017) study) was a spatially extended
110 pattern across the Atlantic ocean with lower SLP roughly following the Gulf Stream front. This result highlighted that
111 atmospheric patterns associated to ~7-yr and ~17-yr variabilities are not similar and these atmospheric patterns exhibit
112 centers of action that are not necessarily corresponding to those of established climate indices such as the NAO.

113

114 Aquifers very often act as low-pass filters, leading to high-amplitude LFV in GWL. Numerous studies also addressed the
115 physical and morphometric parameters controlling the significance of these variabilities in GWL: the superficial formations
116 properties, the vadose zone properties and the aquifers intrinsic properties being the main accountable of their magnitude
117 (Slimani et al., 2009; El Janyani et al., 2012; Velasco et al., 2017; Rust et al., 2018). In Normandy, Slimani et al. (2009) and
118 El Janyani et al. (2012) identified a significant ~7-yr variability in GWL of chalk aquifer. Recently, Baulon et al. (2020) also
119 identified a ~17-yr variability in significant proportion in GWL of some French northern aquifers constituted of chalk and



120 limestones. Therefore, aquifers exhibiting a significant LFV would display highly dependent extreme levels to such
121 variabilities. For instance, Rust et al. (2019) showed that hydrogeological droughts in UK are highly dependent of the ~7-yr
122 variability: the major droughts emerging during low multi-annual levels, excepting the 1975 drought. In addition, Bonnet et
123 al. (2020) described the influence of multi-decadal variability on high and low flows and how it can impact short-term
124 drought events through groundwater-river exchanges in the Seine basin.

125

126 In summary, a few studies concluded to a potential high impact of large-scale climate-induced LFV in supporting high and
127 low GWL, but none of them have yet investigated how much groundwater extremes (GWE) depend on such variability.
128 Throughout the text, for the sake of clarity, GWE will refer to both very high or very low GWL, according to certain
129 thresholds that will be defined in subsequent sections.

130

131 To answer this question, a simple approach based on the decomposition of GWL time series of northern French aquifers into
132 high- to low-frequency components is proposed in this study over the 1976-2019 period. Beforehand, we quantified the
133 variance distribution across timescales for assessing the significance of low-frequency variations in GWL signals,
134 particularly of multi-annual (~7-yr) and decadal (~17-yr) variabilities (Section 4). Then, our methodology consists to
135 evaluate the influence of timescales corresponding to multi-annual and decadal variabilities by filtering one or both
136 timescale(s) from the original signal to assess how their withdrawal affects threshold exceedance. First, we propose
137 estimating the proportion of high (HL) or low levels (LL) associated to the multi-annual or decadal variabilities, and then by
138 the combination of both (Section 5). We also propose determining through a long groundwater time series (106 years of data
139 available) if proportions of HL and LL associated to LFVs are consistent with those obtained in the short term. Second, we
140 propose determining on four well-known historical events the contribution of multi-annual and decadal variabilities in the
141 amplitude of threshold exceedance (ATE) and identify what parameters may control this contribution (Section 6).



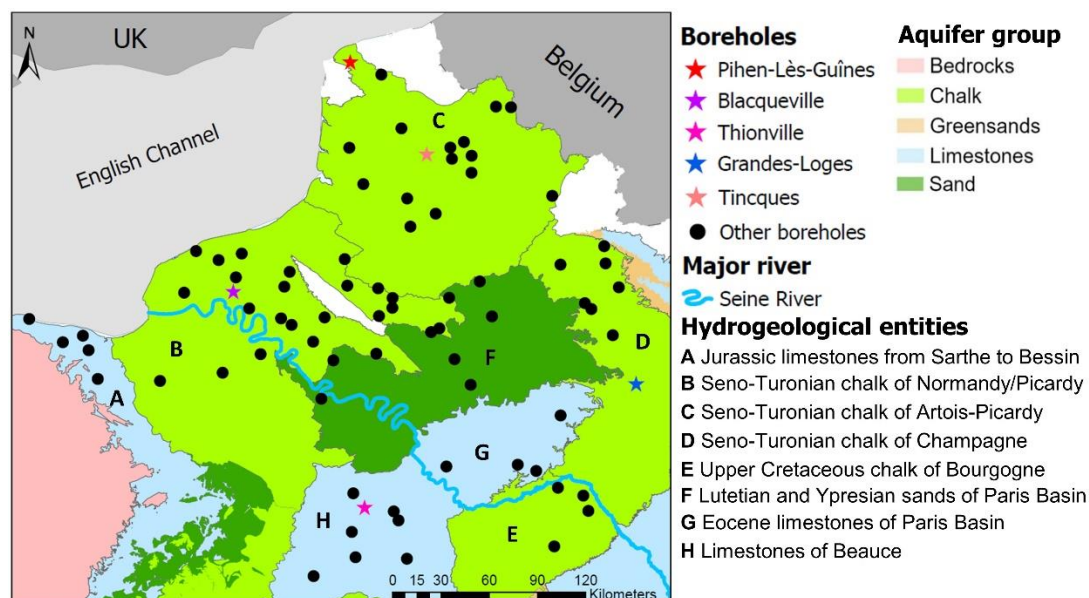
142 2. Effective precipitation and groundwater data

143 For this study, we used 78 boreholes in the Paris Basin (northern France), with GWL time series being little or not affected
144 by pumping (Fig. 1). The study area was restricted to the Paris Basin in order to carry out the analysis over a relatively long
145 period (1976-2019). Boreholes were selected from a BRGM database on boreholes not influenced by human activities
146 (Baulon et al., 2020) that was constituted in three steps:

- 147 (i) a selection of boreholes with time series satisfying criteria of duration, minimum amount of data per
148 month, maximum length of gaps;
- 149 (ii) the crossing of pre-selected boreholes with other BRGM databases on known anthropogenic influences;
- 150 (iii) numerous visualisations of time series with the hydrogeologists responsible for piezometric networks, in
151 order to retain only non-influenced boreholes.

152 Time series of boreholes in this database were initially gathered in the ADES database that contains all groundwater data
153 (quantity and quality) across continental France (<https://ades.eaufrance.fr/>).

154



155

156 **Figure 1: Spatial distribution of the 78 selected boreholes through major hydrogeological entities of the Paris Basin.**

157



158 The criteria satisfied for selecting GWL time series for the present study were:

- 159 • The length of time series must be higher or at least equal to 44 years.
- 160 • The minimum amount of data within a month is set to one monthly datum before the measurement
161 automation and three data after the measurement automation.
- 162 • The length of consecutive gaps must be <3 yr for time series starting after 1950 and <10 yr for time series
163 starting before 1950. This allows time series in the new database to preserve LFV in the data. Several gaps
164 in the time series can be allowed if these criteria are respected, and if the number of gaps and their lengths
165 are small.

166 Before data analysis, a visual check of the GWL time series served to remove or correct erroneous data.

167

168 The analysis of the influence of LFV on HL and LL was conducted over the 1976-2019 period providing the best
169 compromise between the spatial distribution of boreholes and time series length. In this work, all time series had a monthly
170 time step to consider all possible GWL variation types from most reactive to most inertial ones. Then, monthly missing
171 values were filled with linear interpolation to perform spectral analyses.

172

173 GWL time series capture chalky formations, calcareous formations and sandy formations of the Paris Basin. In addition, we
174 also used the GWL time series of Tincques monitoring the Seno-Turonian chalk of Artois-Picardy since 1903 (Fig. 1). This
175 time series allowed us to perform our analysis on a longer temporal perspective and compare results with those obtained on
176 short-term time series.

177

178 Time series of 4 boreholes, among the 78 of the study, were used to introduce the different GWL variation types in Paris
179 Basin aquifers: Pihen-Lès-Guînes, Blacqueville, Thionville, Grandes-Loges (Fig. 1). These boreholes were chosen because
180 each of them is representative of a GWL variation type.

181



182 For the aforementioned boreholes monitoring GWL of chalk aquifers (Pihen-Lès-Guînes, Blacqueville and Grandes-Loges),
183 we also investigated effective precipitation (EP) corresponding to these boreholes. For each borehole, we assigned to it the
184 mesh with EP time series the most explanatory of GWL. This linkage between the borehole and a SAFRAN mesh was
185 carried out prior to this study by correlative analysis. In this study, we used monthly cumulative EP time series over the
186 1976-2019 period.

187

188 The meteorological data (precipitation (P), snow, temperature and Penman-Monteith potential evapotranspiration (PET))
189 from the SAFRAN reanalysis were used as input data to compute effective precipitation. This reanalysis provides daily data
190 on a 8x8km² mesh covering France from 1958 to 2019 (Vidal et al., 2010). The effective precipitation ($EP = P - PET$) were
191 computed using a gridded water budget model with 8km resolution at daily time step. It relies on the water budget method
192 proposed by Edijatno and Michel (1989). The water-budget method considers that in the water cycle, the soil acts as a
193 reservoir characterized by its water storage capacity. Edijatno and Michel (1989) introduced a quadratic law to progressively
194 empty the soil water reserves and to distribute the positive difference between P and PET between EP and soil storage.

195 **3. Methodological approach**

196 **3.1. Characterization of groundwater multi-timescale variability**

197 In order to determine the prominence of LFV in GWL, the maximum overlap discrete wavelet transform (MODWT) analysis
198 was applied. This is an iterative filtering of the time series that uses a series of low-pass and high-pass filters. Consequently,
199 one high-frequency component called “wavelet detail” and one lower frequency component called “approximation” or
200 “smooth” are produced at each timescale. At the next level, the smooth is then subsequently decomposed into another
201 wavelet detail and smooth. The original signal can be rebuilt by summing up all wavelet details and the last smooth. The
202 original signal is then separated into a relatively small number of wavelet components from high- to low frequencies, which
203 together explain the total variability of the signal. Here, we achieved a full decomposition of the time series by applying the
204 filter bank up to a level corresponding to the $\log_2(N)$ where N is the length of the time series. The least-asymmetric



205 (symmlet) wavelet “s20” was used in order to better capture variability at all timescales of sometimes relatively smooth
206 groundwater level time series.

207

208 However, unlike DWT, MODWT was essentially designed to prevent phase shifts in the transform coefficients at all scales
209 by avoiding downsampling – reducing by a factor 2 the number of coefficients – the signal with increasing scales. It results
210 that the computed wavelet and scaling coefficients at each scale remain aligned with the original time series; that is, the
211 variance explained by these coefficients is located where it truly lies in the time series analysed (Percival and Walden, 2000;
212 Cornish et al., 2003; Cornish et al., 2006). While not necessarily essential for signal or image processing or numerical
213 compression, this property is fundamental for physical interpretation of the wavelet details in multiresolution analysis, and
214 has already been used to that purpose in several studies such as Percival and Mofjeld (1997), Massei et al. (2017) and Pérez
215 Ciria et al. (2019).

216

217 The dominant frequency associated with each MODWT wavelet detail was calculated by Fourier transform of each wavelet
218 detail. The MODWT also provides the amount of variance (or energy) explained by each wavelet detail and frequency level.
219 The energy percentage of a given wavelet detail expresses the relative importance of this variability in the total signal
220 variability. As a result, the energy distribution between wavelet details for each borehole in the database can be extracted and
221 mapped.

222

223 Then, we used the Continuous Wavelet Transform (CWT) for visualizing the spectral content of GWL time series of
224 representative boreholes of each GWL variation type in the Paris Basin. CWT is a widely used method for identifying scales
225 of variability in environmental time series (Torrence and Compo, 1998; Labat, 2005; Liesch and Wunsch, 2019). The
226 literature about CWT is very rich and theoretical background along with an application to climatic variables are available in
227 Torrence and Compo (1998). The CWT produces a time-scale (or time-period) contour diagram on which time is indicated
228 on the x-axis, period or scale on the y-axis and amplitude (or variance, or power) on the z-axis.

229



230 These analyses used R packages wmtsa (Constantine and Percival, 2016) and biwavelet (Gouhier and Grinsted, 2012).

231 **3.2. Influence of low-frequency on the occurrence of high and low groundwater levels**

232 The influence of groundwater LFV (multi-annual and decadal) on HL and LL was estimated with the MODWT method for
233 the 78 selected boreholes. As seen in the 3.1. section, summing up all wavelet details and the last smooth rebuild the original
234 signal. Based on this assessment, we subtracted the interest wavelet detail, corresponding to a specific timescale, from the
235 original signal to evaluate its influence on HL and LL (Fig. 2a). This method allowed us to assess whether the withdrawal of
236 multi-annual (~7-yr) and/or decadal (~17-yr) components leads to a different number and level of GWE in the filtered
237 groundwater time series compared to the original series.

238

239 First, HL and LL were identified in original groundwater time series when they exceed thresholds set at the percentile 0.8
240 and 0.2, respectively (Fig. 2a). Such percentiles were selected because they are the optimal thresholds to have a correct and
241 sufficient number of HL and LL on a 44 years period, particularly for time series with inertial GWL variation type. Once
242 these HL or LL have been identified, for each studied time series, details corresponding to multi-annual variability, decadal
243 variability, and both variabilities were successively subtracted from the original signal. From these filtered time series, we
244 evaluated if the subtraction of one given component affected HL peaks or LL peaks as initially identified in the original data.
245 In the case where HL peaks still exceeded the initial threshold, then the subtracted component(s) had little influence on HL
246 emergence. On the opposite, if peaks moved below the initial threshold, then the subtracted component(s) had significant
247 influence on HL emergence. The same assessment was realised with LL peaks.

248

249 For sake of clarity, in this paper the terms “extremes” or “extreme levels” refer to HL above percentile 0.8 and LL below
250 percentile 0.2.

251

252 For each borehole, we calculated a percentage describing the proportion of HL or LL in GWL generated by the considered
253 component(s) (i.e., HL or LL that were no longer considered as such if the component was filtered). This calculation is
254 presented below with HL as instance:



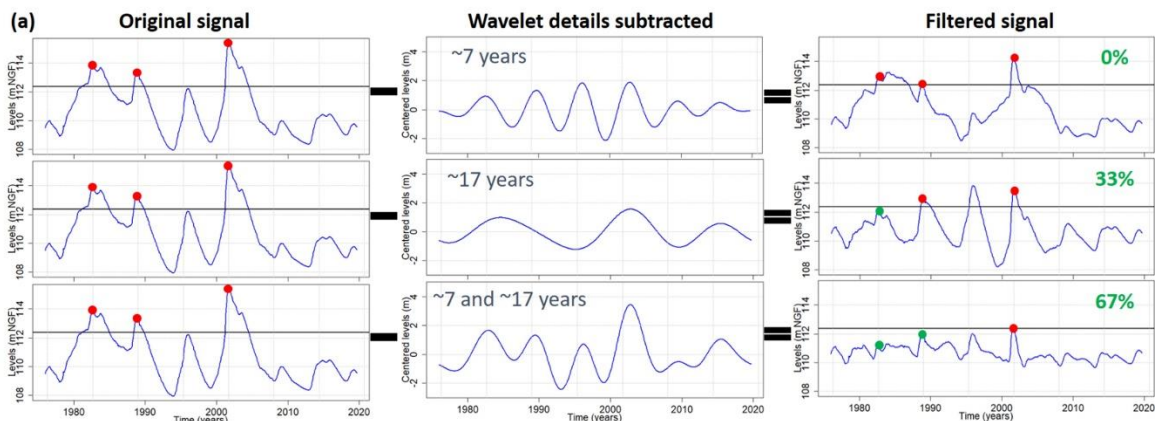
255

256 $Percentage\ of\ HL\ generated\ by\ the\ component = \left(\frac{number\ of\ HL\ moving\ below\ threshold\ in\ filtered\ signal}{number\ of\ HL\ in\ original\ signal} \right) * 100\ (1)$

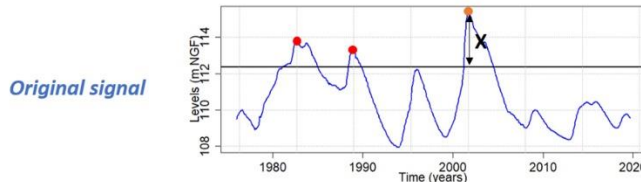
257

258 Then, these results were mapped for each borehole and each filtered component (multi-annual, decadal or both).

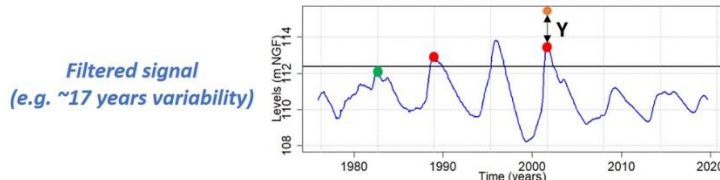
259



(b) **Step 1:** Difference between the reached level (orange) and the threshold in the original signal (= X)



Step 2: Difference between the reached level (orange) in the original signal and the obtained level after filtering (= Y)



Step 3: Contribution of the variability (e.g. ~17 years) in the amplitude of threshold exceedance (%)

$$Contribution\ in\ the\ amplitude\ of\ threshold\ exceedance = \left(\frac{Y}{X} \right) * 100\ (2)$$

260

261 **Figure 2:** Workflow of (a) the influence of low-frequency variability on high and low groundwater levels occurrence (example of

262

high levels); (b) the contribution of low-frequency variability in the amplitude of threshold exceedance. The borehole of

263

Goupillières (chalk of Normandy) is taken as an example.



264 **3.3. Role of groundwater low-frequency variability in the amplitude of threshold exceedance**

265 The calculation of the contribution of groundwater LFV in the amplitude of threshold exceedance (ATE) was achieved with
266 the MODWT method. The methodology consisted in filtering the wavelet details of interest (corresponding to multi-annual
267 and decadal variabilities) to estimate how they impact the amplitude of HL or LL peaks (Fig. 2b).

268

269 First, we estimated the difference between the reached level and the threshold value in the original signal (Fig. 2b; Step 1).
270 Then, we estimated the difference between the reached level in the original signal and the obtained level after filtering the
271 interest detail(s) (Fig. 2b; Step 2). This difference revealed the amplitude of levels carried by the subtracted detail(s). Finally,
272 we estimated the contribution of the filtered component in the amplitude of threshold exceedance with the following
273 equation (Fig. 2b; Step 3):

274
$$\text{Percentage of contribution} = \left(\frac{Y}{X}\right) * 100 \text{ (2)}$$

275 Where Y represented the difference between the observed real level and the obtained level after filtering; X represented the
276 difference between the observed real level and the threshold value.

277

278 From this calculation, 3 types of contribution of multi-annual and/or decadal components were highlighted:

- 279
- 280 • In case of negative percentage, we observed an attenuation of the HL or LL peak owing to the presence of the
281 component considered, meaning that the level reached would have been higher than actually observed without
282 attenuation by this component.
 - 283 • In case of positive percentage lower than 100%, we observed an amplification of the HL or LL peak by the
284 component, meaning that without this component the reached level was lower (HL) or higher (LL) than the actually
285 reached level but still above (HL) or below (LL) the threshold and the HL or LL remained an extreme.
 - 286 • In case of positive percentage higher than 100%, HL or LL peak was generated by the component, meaning that
287 without this component the reached level fall below (HL) or above (LL) the threshold and the HL/LL was no longer
288 considered as an extreme.



289 This analysis allowed us to better understand the contribution of the LFV in the emergence of HL and LL and estimate its
290 contribution in HL/LL amplitude. It was conducted on major HL/LL events of Paris Basin: 1995 and 2001 for HL, 1992 and
291 1998 for LL. We focused precisely on these four events because they are currently among the most severe hydrogeological
292 droughts and floods events across the Paris Basin (Deneux and Martin, 2001; Machard de Gramont and Mardhel, 2006;
293 Seguin et al., 2019). Knowing that the establishment of GWL droughts may occur a few years apart between two boreholes
294 (even in the same hydrogeological entity), we detected the LL peaks on a window extending of more or less 3 years before
295 and after the 1992 and 1998 events to be sure to correctly consider the lowest level.

296 **4. Multi-timescale variability of groundwater levels in aquifers of the Paris Basin**

297 Across the Paris Basin, various types of GWL variation were highlighted depending on the hydrogeological entity
298 considered, according to the dominant time-scale components which characterize their variability (Fig. 3). The Beauce
299 limestones (entity H) consist the most inertial system amongst entities of Paris Basin with a large predominance of decadal
300 variability (DV; purple in Fig. 3). This DV is also significant and even predominant in southern Lutetian and Ypresian sands
301 of Paris Basin (F) and the southern Seno-Turonian chalk of Normandy (B). Farthest north in these two hydrogeological
302 entities, the importance of the DV shrinks to be present in almost equal proportion with the multi-annual variability (MAV;
303 darkblue in Fig. 3). The MAV becomes predominant in the northern Seno-Turonian chalk of Normandy/Picardy (B). From
304 eastern Seno-Turonian chalk of Normandy/Picardy (B) to northern Seno-Turonian chalk of Artois-Picardy (C), the MAV
305 constitutes a half to a quarter of total variability, while the DV diminishes significantly in the Artois-Picardy basin.

306

307 On the opposite, the annual variability (AV; pink in Fig. 3) swells from eastern Seno-Turonian chalk of Normandy/Picardy
308 to Artois-Picardy to represent up to a quarter of total groundwater variability (Fig. 3). The AV is also significant, and even
309 predominant compared to MAV and DV, in GWL of Champagne and Bourgogne chalk (D and E). These entities exhibit the
310 most reactive water tables in our study.

311

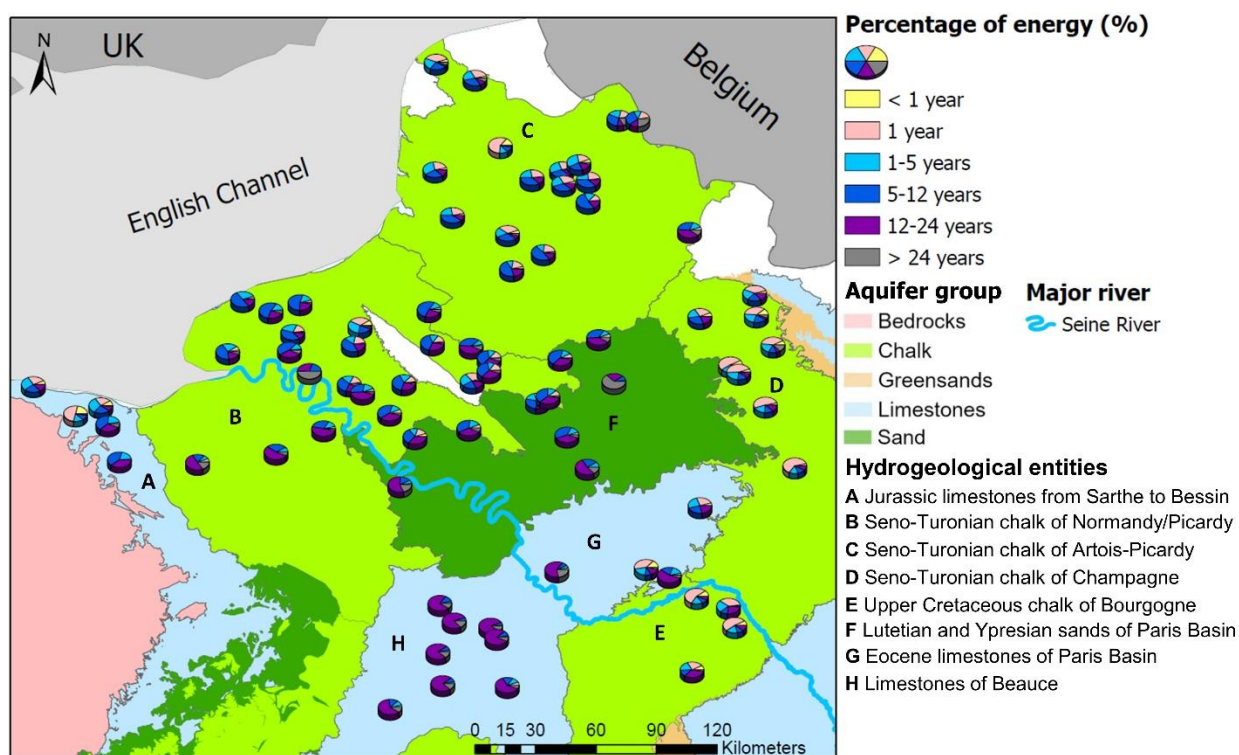


312 Finally, the Jurassic limestones of Bessin (A) exhibit two types of GWL variation: inertial farthest south with predominant
313 MAV and DV, and more reactive on the border of English Channel with AV and inter-annual variability (light blue in Fig. 3)
314 accounting for a half of total variability.

315

316 No typical GWL variation was identified in the Eocene limestones of Paris Basin (G; Fig. 3).

317



318

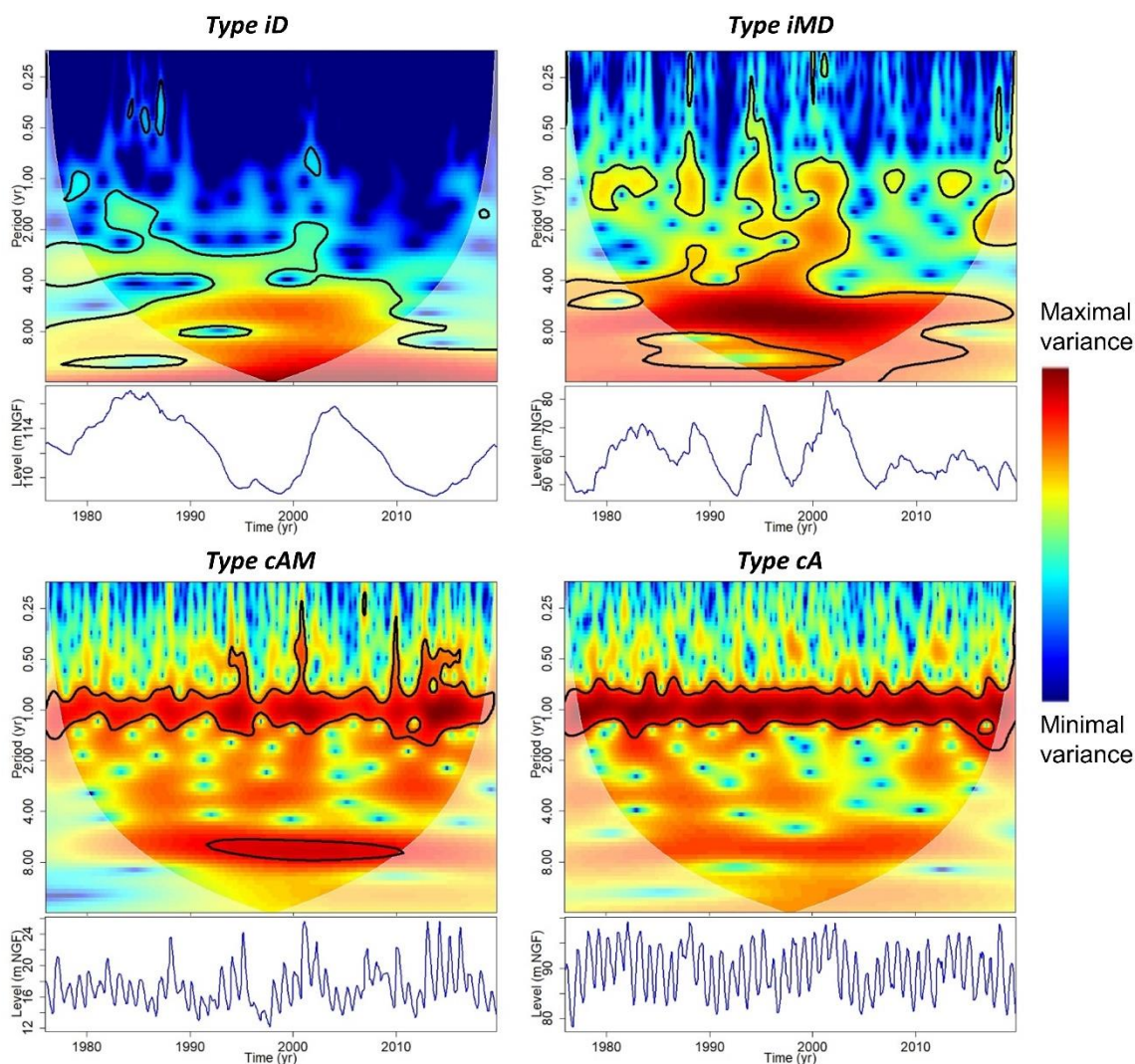
319 **Figure 3: Multi-timescale variability of groundwater levels in Paris Basin (78 boreholes). Pie charts describe the energy percentage**
320 **of each timescale of variability reflecting their importance in total groundwater level variations.**

321 Overall, hydrogeological entities in the Paris Basin display 4 major types of GWL variation:

- 322 • Type iD: inertial with a predominant Decadal variability such as entity H (Fig. 3 and 4)
- 323 • Type iMD: inertial with predominant Multi-annual and Decadal variabilities such as entities B, F and southern part
324 of entity A (Fig. 3 and 4)



- 325 • Type cAM: combined with predominant Annual and Multi-annual variabilities such as entity C (Fig. 3 and 4)
- 326 • Type cA: combined with a predominant Annual variability such as entities D and E (Fig. 3 and 4)
- 327



328

329 **Figure 4: Time series (bottom) and wavelet spectra (up) of a typical time series representing each major groundwater level**

330 **variation type. For type iD, this is the time series of Thionville borehole (Beauce limestones – entity H); for type iMD, Blacqueville**

331 **borehole (chalk of Normandy – entity B); for type cAM, Pihen-Lès-Guînes borehole (chalk of Artois-Picardy – entity C); and for**

332 **type cA, Grandes-Loges borehole (chalk of Champagne – entity D).**



333 **5. Influence of low-frequency variability on the occurrence of high and low groundwater levels**

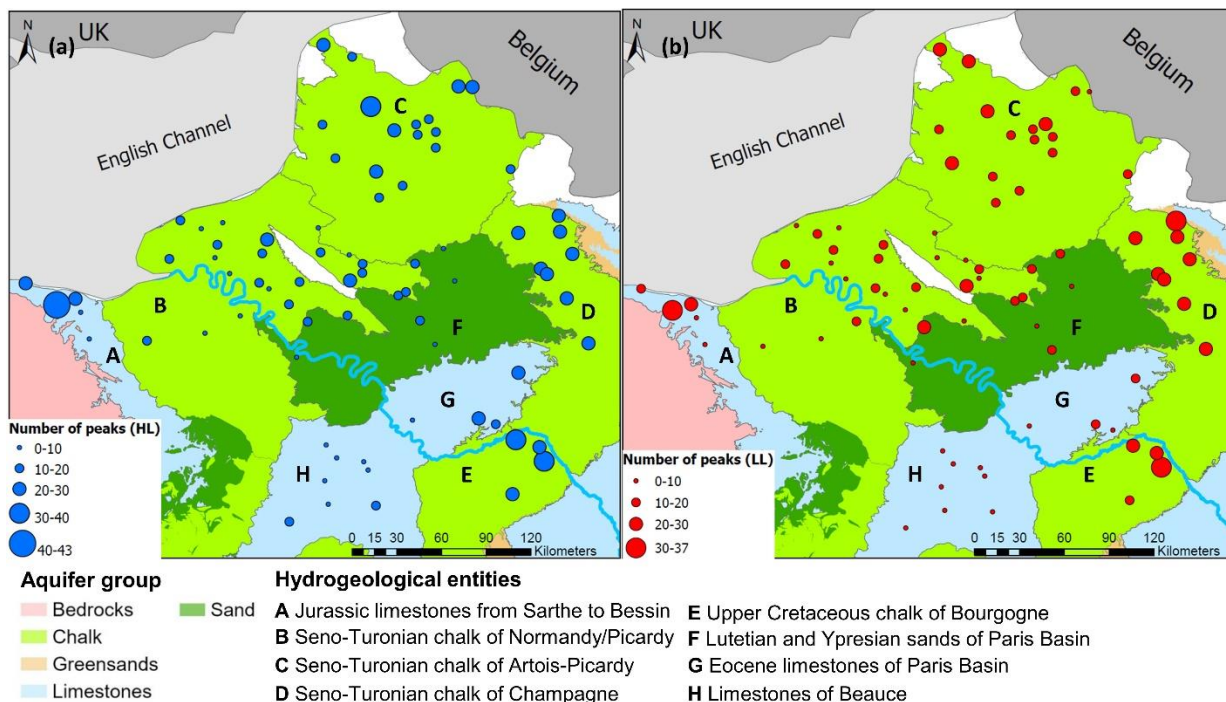
334 **5.1. Spatial distribution across the Paris Basin**

335 This section aims determining to what extent the LFV influences the quantity of HL and LL in groundwater time series over
336 the 1976-2019 period and what percentage amongst these extreme levels were generated by the MAV (~7-yr), the DV (~17-
337 yr) and the combination of both.

338

339 Figure 5 displays for each groundwater time series the number of HL peaks above a threshold set on the percentile 0.8 and
340 LL peaks below a threshold set on the percentile 0.2 through hydrogeological entities of Paris Basin. Types iD and iMD
341 entities displayed the lowest number of HL and LL peaks with a decadal occurrence (H) or a multi-annual occurrence (B, F,
342 southern A). Conversely, the quantity of HL and LL increased significantly in types cAM and cA entities with a quasi-
343 annual occurrence throughout multi-annual HL and multi-annual LL, respectively (entities C, D, E, and northern A). These
344 results highlighted the significant control of the LFV on the number of HL and LL peaks: the more the LFV is predominant
345 in GWL, the more the number of peaks is reduced because they are supported by this LFV, which naturally contains a few
346 extremes over a relatively short period of only a few decades.

347



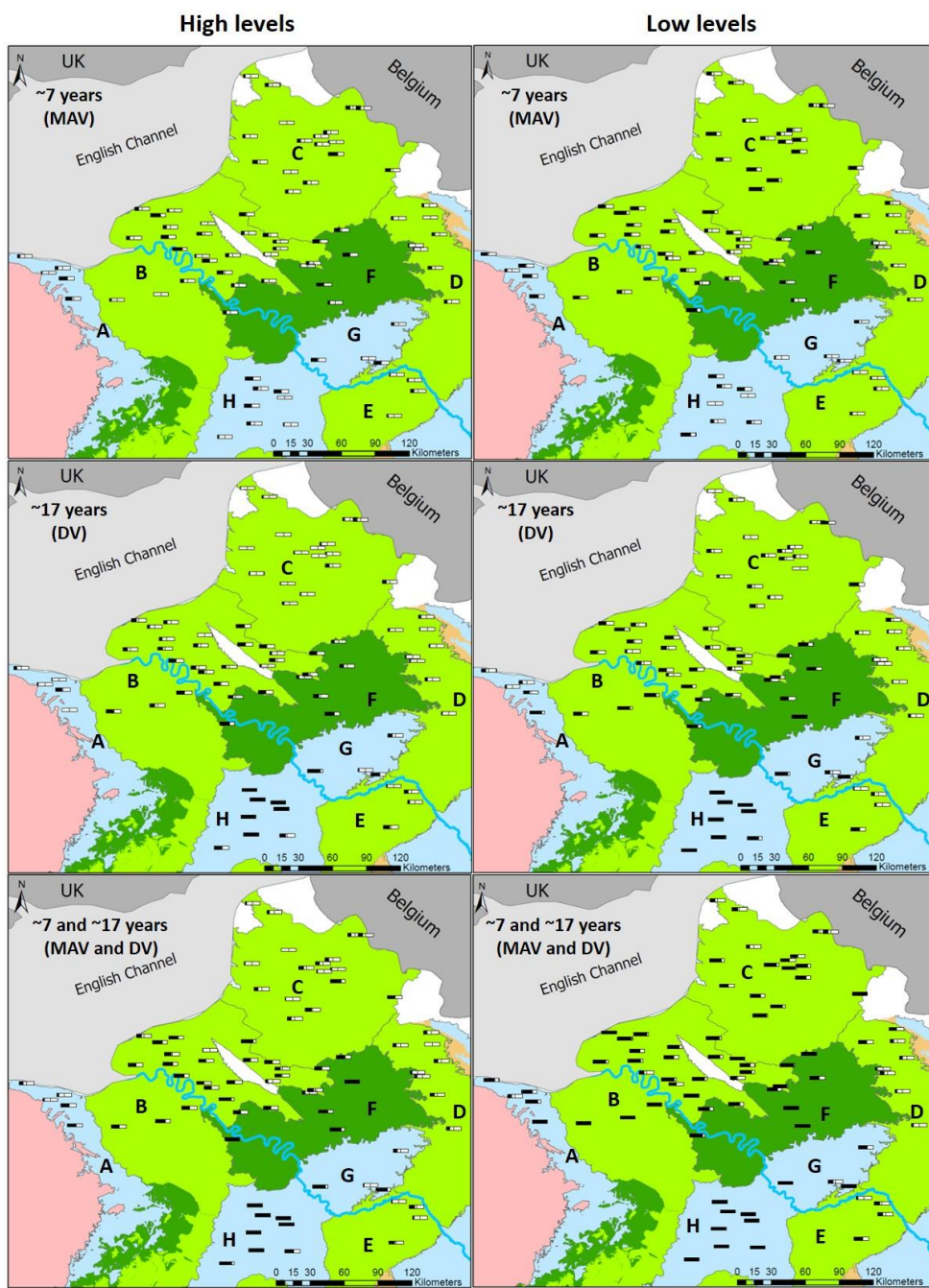
348

349 **Figure 5: Number of HL peaks above percentile 0.8 (a); and LL peaks below percentile 0.2 (b) over the 1976-2019 period.**

350

351 Amongst these HL and LL peaks, we estimated for each groundwater timeseries what percentage of HL and LL are
 352 generated by MAV, DV and both variabilities (Fig. 6). The percentage of HL and LL generated by a given variability was
 353 closely related to the GWL variation type in hydrogeological entities.

354





356 **Figure 6: Percentage of HL or LL generated by the ~7-yr (MAV), ~17-yr (DV), ~7-yr and ~17-yr components in hydrogeological**
357 **entities of Paris Basin. This percentage corresponds to the proportion of HL or LL that are not considered as extreme levels (being**
358 **respectively below or above threshold) when the component(s) is (are) absent from the original signal, meaning that these HL or**
359 **LL are significantly supported by the component.**

360

361 For the type iD entity (H), the DV generated 100% of HL and LL. Exceptions were noticeable for the two southernmost
362 boreholes that might be related to the weaker significance of the DV in GWL.

363

364 For type iMD entities (B, F, southern A), the LFV had a lesser influence on both HL and LL. The combination of both
365 variabilities (MAV and DV) explained the emergence of at least 50% of LL. This was also often the case for HL but in lesser
366 proportions. Individually, the MAV and DV still explained a rather large proportion of HL and LL.

367

368 For the type cAM entity (C), the influence of LFVs on GWE was reduced compared to types iD or iMD entities, particularly
369 on HL. A larger proportion of LL than HL was influenced by the LFV. Indeed, less than 50% of HL were generated by the
370 combination of MAV and DV. Conversely, more than 50% of LL were generated by the combination of MAV and DV in
371 southern C. In the northern part, the proportion approached the 50% although it did not exceed it. This significant proportion
372 of LL generated by the combination of both variabilities seemed to be directly related to the influence of the MAV.

373

374 For type cA entities (D and E), the proportion of HL and LL generated by the LFVs was relatively small. Individually, the
375 MAV and DV explained the emergence of less than 50% of HL and LL identified in the time series. The combination of
376 both variabilities did not allow either to explain the emergence of more than 50% of HL and LL.

377

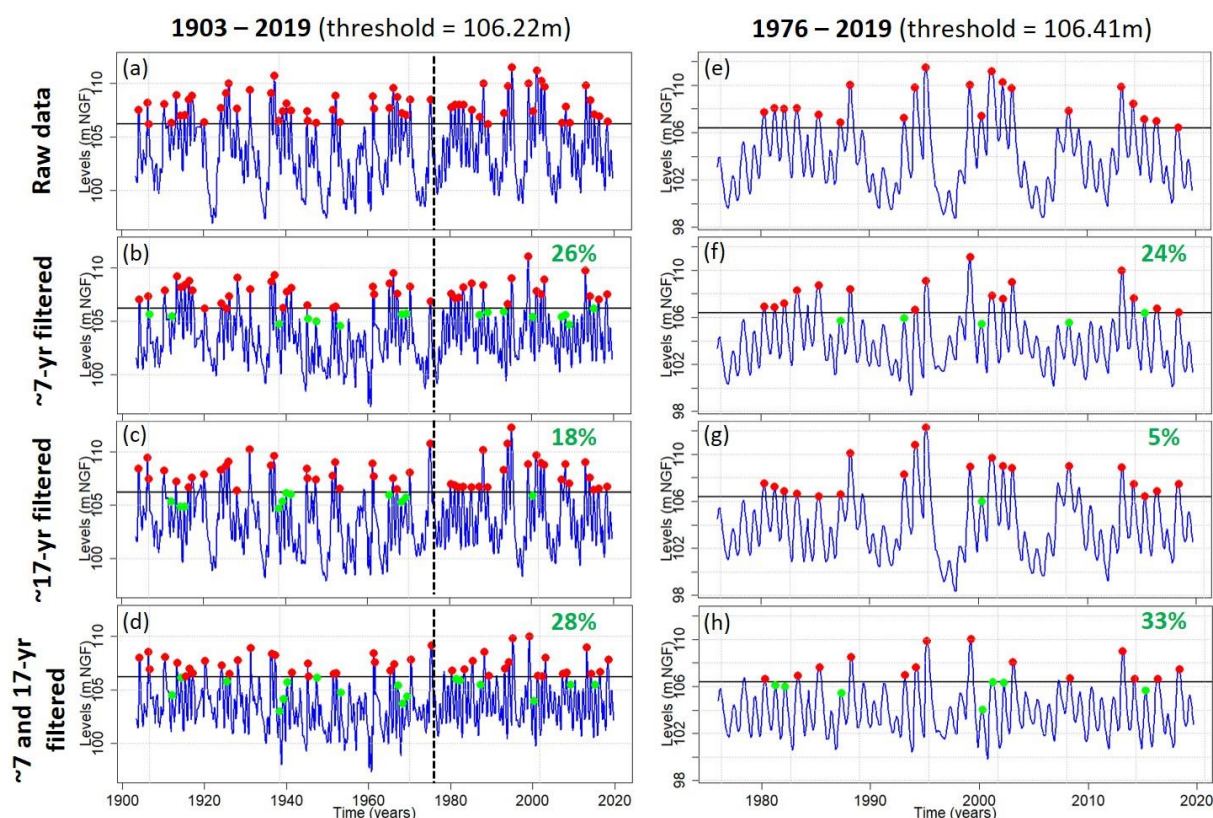
378 Overall, the LFVs seemed to have a larger influence on LL than HL.



379 **5.2. One century of high and low groundwater levels and low-frequency variations**

380 The time series used previously for assessing the spatial distribution of high and low GWL as controlled by LFV are rather
381 short, banning any assessment of long-term variations of high- and low GWL. To explore it, the same analysis than in
382 section 5.1. was conducted for the borehole of Tincques monitoring the Seno-Turonian chalk of Artois-Picardy (entity C)
383 and providing data since 1903 (Fig. 7 and 8).

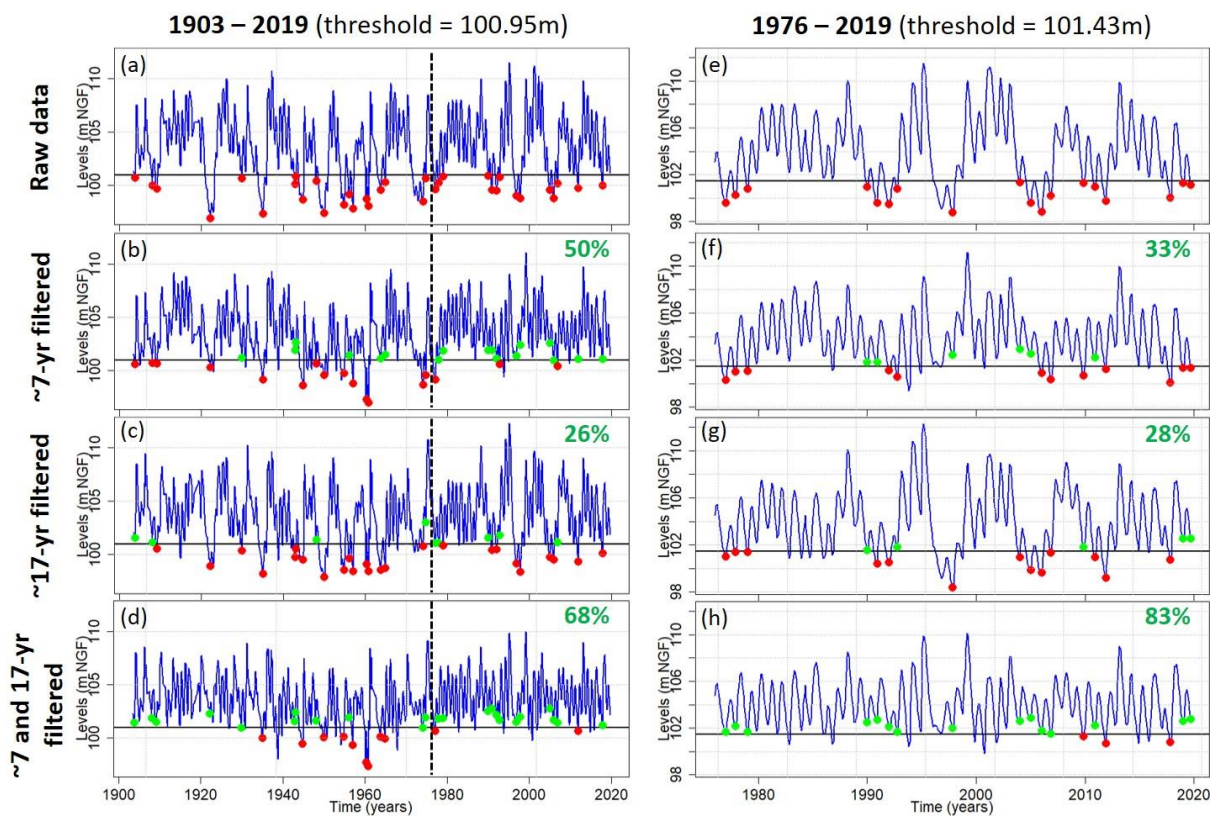
384



385

386 **Figure 7: Influence of ~7-yr (MAV), ~17-yr (DV), ~7-yr and ~17-yr variabilities on the occurrence of HL for the Tincques' GWL**
387 **over the 1903-2019 and 1976-2019 periods. The percentage of HL generated by the filtered component(s) (i.e., moving below the**
388 **percentile 0.8) is indicated in green. The dotted black line represents the 1976 year.**

389



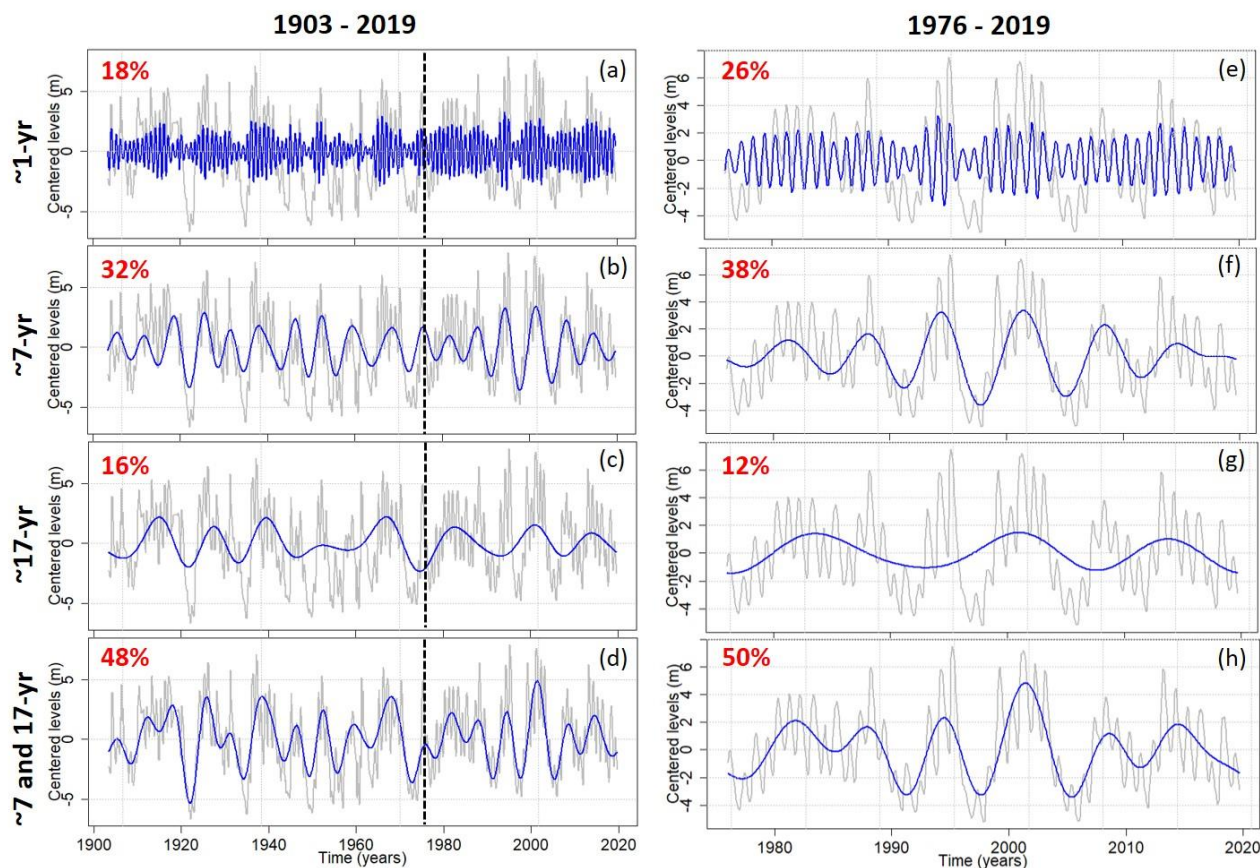
390

391 **Figure 8: Influence of ~7-yr (MAV), ~17-yr (DV), ~7-yr and ~17-yr variabilities on the occurrence of LL for the Tincques' GWL**
392 **over the 1903-2019 and 1976-2019 periods. The percentage of LL generated by the filtered component(s) (i.e., moving above the**
393 **percentile 0.2) is indicated in green. The dotted black line represents the 1976 year.**

394

395 The predominant components of GWL variability were extracted and plotted on figure 9 for both 1976-2019 and 1903-2019
396 periods. On the long-term (1903-2019), the combination of MAV and DV explained ~50% of GWL total variance, that was
397 consistent with the percentage obtained on the short term for Tincques time series but also for the others GWL time series in
398 the South part of entity C (Fig. 9 and 3).

399



400

401 **Figure 9: Maximum overlap discrete wavelet transform (modwt) of groundwater levels at Tincques in the Seno-Turonian chalk of**
402 **Artois-Picardy over the 1903-2019 and 1976-2019 periods. In grey is displayed the original time series, in blue the wavelet detail, in**
403 **red the energy percentage.**

404

405 First, the identified thresholds (i.e., percentiles 0.8 and 0.2) were lower on the longer period (1903-2019) than the shorter one
406 (1976-2019) indicating lower GWL in average and more severe hydrogeological droughts before the 1970s (Fig. 7 and 8).

407

408 The proportions of HL and LL generated by the MAV, DV, and the combination of MAV and DV on both periods for
409 Tincques (1976-2019 and 1903-2019) were compliant to the ranges of percentages exhibited by boreholes monitoring the
410 Seno-Turonian chalk of Artois-Picardy over the 1976-2019 period (Fig. 7, 8 and 6). Similarly to the previous conclusions,
411 we also observed a higher influence of LFVs on LL than HL (Fig. 7 and 8).



412

413 Some HL that fell below threshold when the MAV or DV was filtered out from the original signal – and then being no
414 longer considered as GWE – did not fall below the threshold when both MAV and DV were filtered out, remaining GWE
415 (Fig. 7). As instance, we can observe such phenomenon for the 3rd HL on the 1903-2019 period (Fig. 7b and 7d). This is
416 related to the compensation between both MAV and DV: the withdrawal of DV increased the level compared to raw data
417 (Fig. 7c and 7a), much more than the level decreased when the MAV was filtered out (Fig. 7b and 7a), therefore the level
418 stayed above the threshold when both variabilities were filtered out (Fig. 7d). The same phenomenon is visible for some LL
419 as well (Fig. 8).

420

421 Proportions of HL generated by the MAV (Fig. 7b and 7f) or the combination of MAV and DV (Fig. 7d and 7h) were close
422 between both periods (1976-2019 and 1903-2019). Over the 1903-2019 period, the HL generated by the MAV (Fig. 7b) or
423 the combination of MAV and DV (Fig. 7d) were regularly distributed over time. Conversely, the proportion of HL generated
424 by the DV was much higher for the 1903-2019 period (Fig. 7c) than the 1976-2019 period (Fig. 7g), the DV having
425 seemingly much more influence on HL before the 1980's.

426

427 LL peaks were found to be much more pronounced before the 1960's (Fig. 8a). The lowest level in 1921 was significantly
428 supported by the combination of MAV and DV (Fig. 8d and 9d). The LL between ~1930 and ~1970 remained present even
429 when both MAV and DV were removed (Fig. 8d). A multi-decadal LL period between ~1930 and ~1970, supporting the LL
430 peaks, explained why the proportion of LL generated by the combination of both variabilities on the 1903-2019 period (Fig.
431 8d) was much lower than the one displayed on the 1976-2019 period (Fig. 8h). The DV generated a similar proportion of LL
432 for both studied periods (Fig. 8c and 8g). Finally, the proportion of LL generated by the MAV was larger over the 1903-2019
433 period (Fig. 8b) than the 1976-2019 period (Fig. 8f), with the majority of LL generated by this variability emerging since the
434 1960's.



435 **6. Contribution of groundwater low-frequency variability to the emergence of well-know historical events**

436 The following subsections aim determining the contribution of either MAV or DV or both of them in the emergence of
437 historical events: 1995 and 2001 for HL, 1992 and 1998 for LL (Fig. 10 and 11). This study was based on a percentage of
438 contribution of the ~7-yr (MAV), ~17-yr (DV) or ~7 and ~17-yr components in the ATE. Three results can be reached: an
439 attenuation of the HL or LL peak by the component when the percentage is <0% (i.e., the level was higher (HL) or lower
440 (LL) than original level when the component was filtered); an amplification of the HL or LL peak by the component when
441 the percentage is between 0% and 100% (i.e., the level was lower (HL) or higher (LL) than original level when the
442 component was filtered but staying above (HL) or below (LL) the threshold and remaining an extreme); the generation of the
443 HL or LL peak by the component when the percentage is $\geq 100\%$ (i.e., the level was no longer considered as an extreme
444 when the component was filtered moving below (HL) or above (LL) the threshold).

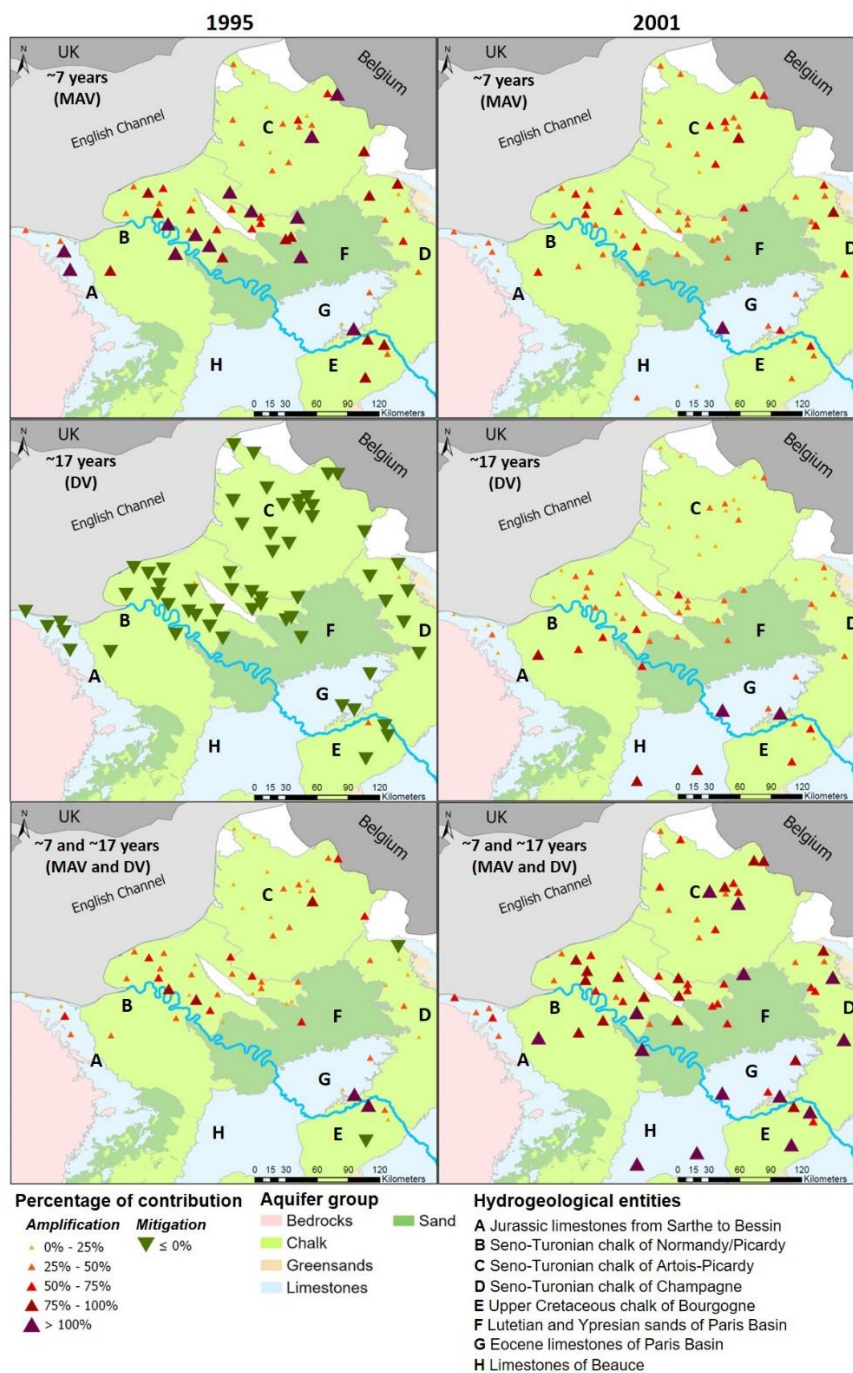
445

446 In addition, figure 12a displays for 3 boreholes representative of each GWL variation type of chalk aquifers (type iMD –
447 Blacqueville, type cAM – Pihen-Lès-Guînes, type cA – Grande-Loges) the modwt extraction of AV (~1-yr), MAV (~7-yr),
448 DV (~17-yr), MAV and DV (~7-yr and ~17-yr) with the studied historical events highlighted. It provides a visual insight of
449 the situation (i.e., positive or negative level) of these variabilities during the emergence of historical events. The same
450 extraction is also realised in EP to be compared to GWL (Fig. 12b).

451

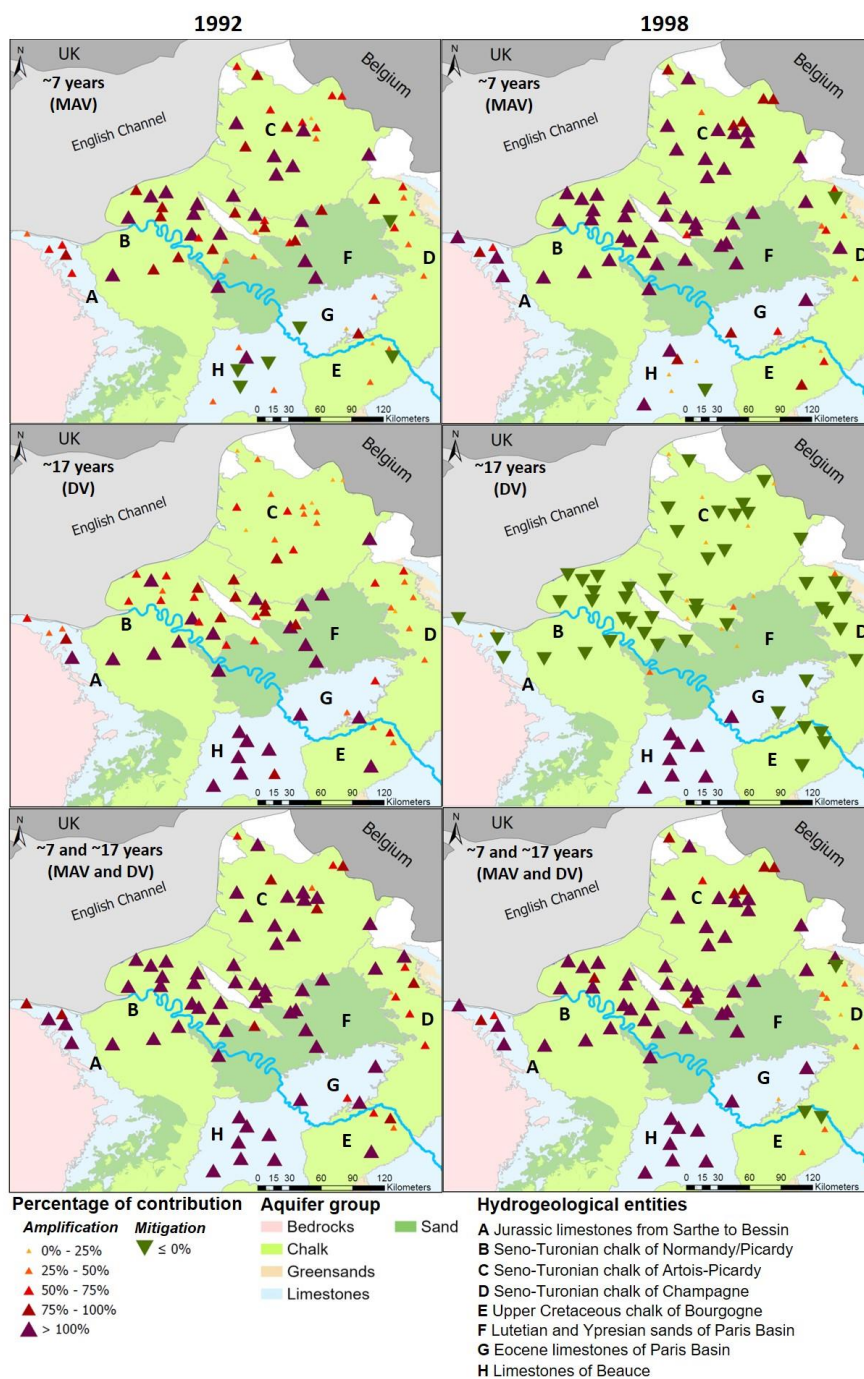
452 In the subsequent section, the term “concomitant situation” refers to concomitant minima or concomitant maxima levels of
453 MAV and DV. The term “opposite situation” refers to maxima-minima or minima-maxima levels of MAV and DV.

454



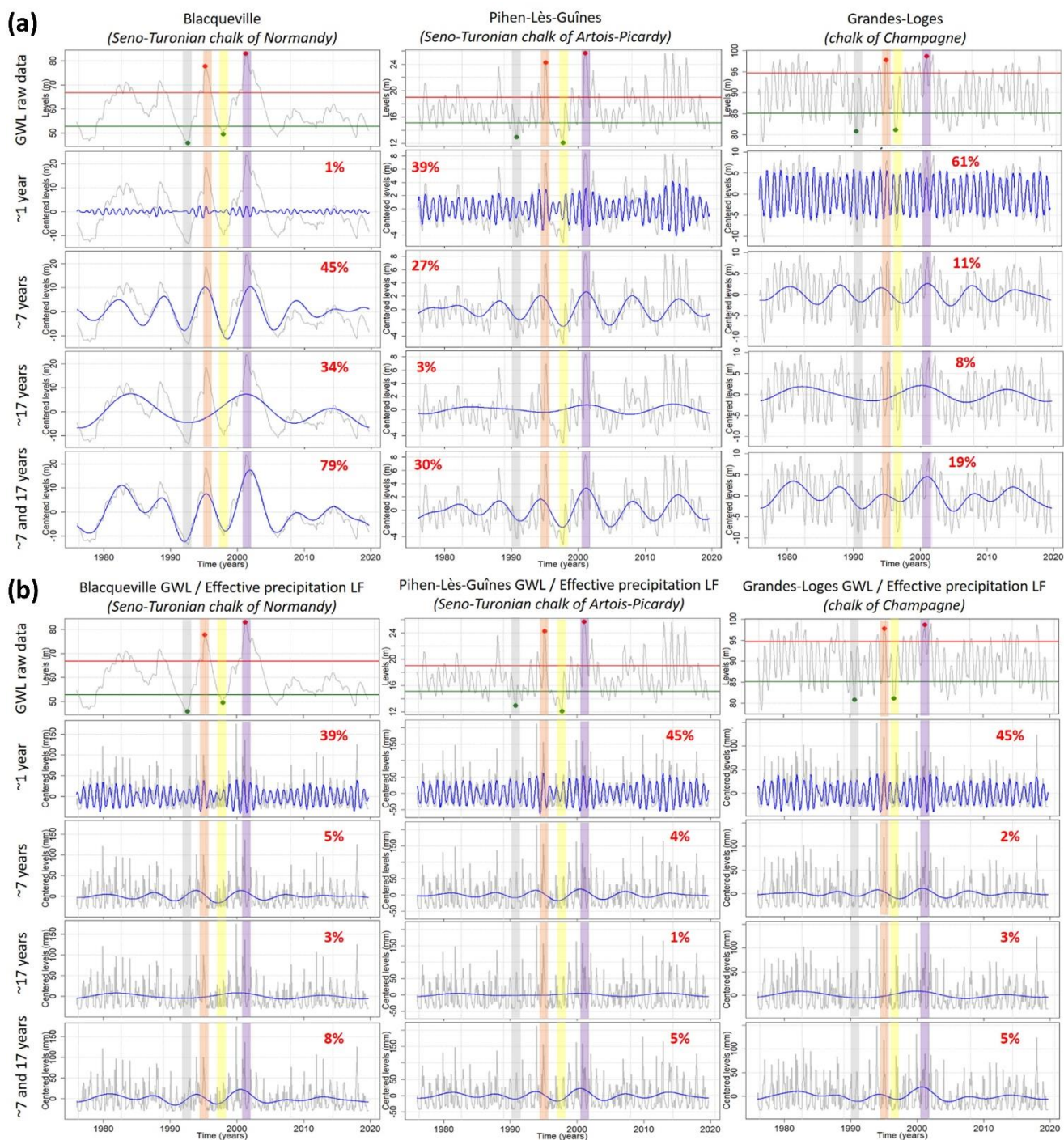
455

456 **Figure 10: Contribution of ~7-yr (MAV), ~17-yr (DV), ~7-yr and ~17-yr components in the amplitude of threshold exceedance**
 457 **(ATE): case of 1995 and 2001 high levels (percentile 0.8). It indicates if the component generates (contribution in ATE ≥ 100%),**
 458 **attenuates (contribution in ATE < 0%) or amplifies (contribution in ATE between 0% and 100%) the high level. In case of missing**
 459 **borehole(s) on maps, it means that either the 1995 or 2001 high level was not identified in the time series (i.e. no threshold**
 460 **exceedance).**



461

462 **Figure 11: Contribution of ~7-yr (MAV), ~17-yr (DV), ~7-yr and ~17-yr components in the amplitude of threshold exceedance**
 463 **(ATE): case of 1992 and 1998 low levels (percentile 0.2). It indicates if the component generates (contribution in ATE ≥ 100%),**
 464 **attenuates (contribution in ATE < 0%) or amplifies (contribution in ATE between 0% and 100%) the low level. In case of missing**
 465 **borehole(s) on maps, it means that either the 1992 or 1998 low level was not identified in the time series (i.e. no threshold**
 466 **exceedance).**



467

468 **Figure 12: Extraction of ~1-yr (AV), ~7-yr (MAV), and ~17-yr (DV) components in (a) groundwater levels of three boreholes**
 469 **monitoring chalk aquifers and in (b) effective precipitation corresponding to the three boreholes. The 1992 low level is highlighted**
 470 **in grey, the 1995 high level in orange, the 1998 low level in yellow, the 2001 high level in purple. The energy percentage of each**
 471 **component or association of components is indicated in red.**



472 **6.1. The low-frequency origin of the selected historical events**

473 The low-frequency origin of each historical event was spatially consistent across aquifers of the Paris Basin (Fig. 10 and 11).
474 First, the 2001 HL and the 1992 LL resulted of a concomitant situation of MAV (~7-yr) and DV (~17-yr), both leading to the
475 accentuation of the amplitude of the extreme level observed. Figure 12a also highlights such situations for both events via
476 the MODWT analysis of GWL for three boreholes in the chalk. Conversely, the 1995 HL and the 1998 LL resulted of an
477 opposite situation of the MAV and DV, leading to the attenuation of the extreme level (Fig. 10 and 11). Indeed, the 1995 HL
478 originated from a multi-annual HL attenuated by a decadal LL, while the 1998 drought originated from a multi-annual LL
479 attenuated by a decadal HL (Fig. 12a).

480

481 We also found such concomitant or opposite situations of MAV and DV in Effective Precipitation (Fig. 12b). The presence
482 of such variabilities in EP indicates their climatic origin. Cross-correlation in figure 13 indicated that such LFBs in GWL
483 lagged those in EP from 0 month for the most reactive system (chalk of Champagne – Type cA) to 1.3 years for the most
484 inertial system (Seno-Turonian chalk of Normandy – Type iMD).

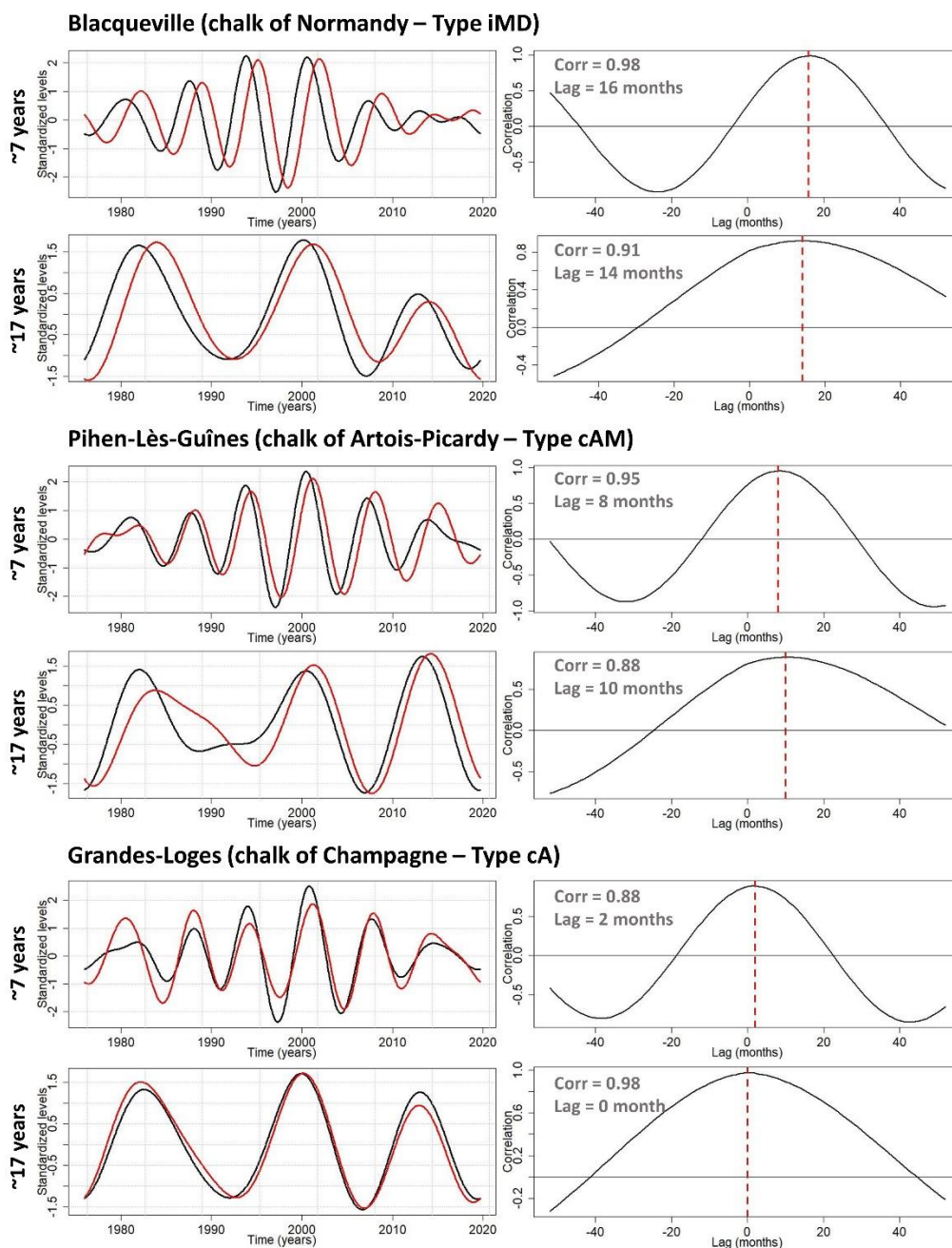
485

486 Although such concomitant or opposite situations of MAV and DV in GWL were overall consistent within and between the
487 hydrogeological entities, some discrepancies can be highlighted locally. The influence of the DV during the 1998 drought is
488 a typical example: while it attenuated LL, it also sporadically amplified LL in some places (entities A, B, C, D, F, G and H in
489 Fig. 11). Such discrepancies might be explained by local basin properties that may operate different filtering effects. This
490 phenomenon was particularly recurring in GWL of entity H, and this is developed in section 6.2.1.

491

492 In addition, the contribution of each component to the ATE differed according to hydrogeological entities and the GWL
493 variation type (Fig. 10 and 11). Therefore, the subsequent section aims assessing the specific contribution of MAV and DV
494 to explain the amplitude of HL and LL for each hydrogeological entity.

495



496

497 **Figure 13: Multi-annual (~7-yr - MAV) and decadal (~17-yr - DV) components of effective precipitation (black) and groundwater**
 498 **levels (red) in chalk aquifers of Paris Basin (left side); Cross-correlation between MAV and DV components of effective**
 499 **precipitation and groundwater levels (right side).**



500 **6.2. Contribution of low-frequency variabilities to amplitude of threshold exceedance**

501 **6.2.1. Type iD (inertial – decadal dominant) hydrogeological entities**

502 Entity H displayed the largest contribution of the LFV (i.e., the combination of MAV and DV) in the HL and LL emergence
503 (Fig. 10 and 11). In such typical behaviour with a large predominance of the DV in GWL, the LFV was involved for at least
504 100% in the ATE and always generated the HL or LL, regardless the event. This contribution is primarily related to the DV
505 that alone is responsible for at least 75% of the ATE. During the 1998 LL, the DV in entity H displayed an opposite
506 influence to that of other hydrogeological entities (Fig. 11). While the DV primarily attenuated the LL peak for the other
507 entities, it generated the LL peak in entity H. Indeed due to its large predominance in GWL, the DV can never attenuate LL
508 (or HL) peaks because this component supports exclusively the HL and LL peaks.

509 **6.2.2. Type iMD (inertial – multi-annual and decadal dominant) hydrogeological entities**

510 Such entities (B, F, southern A) exhibited a significant contribution of the LFV (i.e., the combination of MAV and DV) in
511 the HL and LL emergence (Fig. 10 and 11). During the 2001 HL, the LFV was involved for at least 50% in the ATE and this
512 originated from MAV and DV which were both involved in rather similar proportions (Fig. 10). During the 1995 HL, the
513 contribution of the LFV was more reduced due to the attenuation of the HL peak by the DV, and the threshold exceedance
514 was related primarily to the MAV accounting for at least 50% of the ATE (Fig. 10).

515

516 During the drought events, the contribution of the LFV was enhanced as it generated the LL events (Fig. 11). For the 1992
517 drought, the MAV and DV individually accounted for at least 50% in the ATE and may even have generated the LL peak.
518 While this event was generated primarily by the combination of a multi-annual and a decadal LL, conversely the 1998
519 drought was generated by the MAV alone.

520

521 For the four historical events, this is primarily the MAV that drove GWL and guided the reach of a LL or a HL (Fig. 12a;
522 Blacqueville). Due to its large amplitude in GWL over the 1990-2010 period, the highest or lowest levels (over 1976-2019)
523 were reached often during this period. Simultaneously, the DV amplified or attenuated the reached HL or LL. The
524 significance of this attenuation or amplification is directly controlled by the importance of DV in GWL but also by its phase.



525 Hence, the greater the component accounts for a significant part in total GWL variability, the greater the attenuation or
526 amplification. The potential dephasing and distortion of the component induced by the physical and morphometric properties
527 of catchments may also influence on the significance of the attenuation or amplification. The more the HL on the top of
528 decadal HL or the LL in the concavity of decadal LL, the more the amplification. And the more the LL on the top of decadal
529 HL or the HL in the concavity of decadal LL, the more the attenuation.

530

531 The capability of these hydrogeological entities to exhibit a significant DV in GWL, that is responsible for the amplification
532 or the attenuation of HL and LL, induced that the lowest and the highest levels (in raw data) were not necessarily reached
533 during the lowest and highest multi-annual levels (Fig. 12a; Blacqueville). For instance, the lowest level in the raw data was
534 not reached in 1998 when the MAV exhibited its lowest level since the DV in positive phase attenuated this low level, but it
535 was reached in 1992 when the low multi-annual level was less severe but accentuated by the low decadal level. Therefore in
536 such systems, the severity of droughts and HL depends on both MAV and DV.

537 **6.2.3. Type cAM (combined – annual and multi-annual dominant) hydrogeological entities**

538 For the entity C, the LFV (i.e., the combination of MAV and DV) was significantly involved in the LL emergence, while it
539 was more weakly involved in the HL emergence (Fig. 10 and 11). The 1995 HL exhibited the lowest contribution of the LFV
540 due to the opposite situation of MAV and DV (multiannual HL vs decadal LL; Fig. 10). Consequently, LFV was involved
541 primarily for less than 50% in the ATE. Conversely, due to the concomitant maxima of MAV and DV during the 2001 HL,
542 the contribution of LFV was enhanced accounting for 25% to 75% in the ATE (Fig. 10). During drought events, the LFV
543 was much more involved accounting for at least 75% in the ATE and may even have generated the LL (Fig. 11).

544

545 The DV being poorly significant in GWL of the entity C, it was therefore consistent to observe a weak contribution of this
546 variability in the emergence of the 1992 LL and the 2001 HL (Fig. 10 and 11). Conversely, the MAV was more involved
547 because this is the predominant LFV in GWL. In the southern C, the MAV alone generated both LL events (Fig. 11).

548



549 The weak DV in GWL did not allow HL and LL to be significantly attenuated or accentuated. In the entity C, the amplitude
550 of a LL or HL was directly dependent on the amplitude of the MAV (without considering the AV) (Fig. 12a; Pihen-Lès-
551 Guînes). For instance, the lowest level in raw data occurred in 1998 when the MAV exhibited its lowest level, and the 1992
552 LL was less severe like in the MAV. Therefore in such systems, the severity of droughts are almost only dependent on the
553 MAV. In contrast, the severity of HL depends on both MAV and AV.

554 **6.2.4. Type cA (combined – annual dominant) hydrogeological entities**

555 Entities D and E generally displayed the slightest contribution of the LFVs in the HL and LL emergence (Fig. 10 and 11).

556

557 Generally, the contribution of the LFV (i.e., the combination of MAV and DV) in the ATE remained lower than 100% for
558 the four events. Locally, this contribution was higher than 100% and generated the HL or LL. However, it remained rather
559 rare at the scale of these two hydrogeological entities. The highest contributions of the LFV in the ATE were found during
560 events displaying concomitant situation of the MAV and DV (Fig. 10, 11 and 12a – Grandes-Loges). Indeed during the 2001
561 HL and the 1992 LL, the LFV explained at least 50% of the ATE. Conversely, the LFV explained less than 50% of the ATE
562 for events displaying an opposite situation of MAV and DV (1995 HL and 1998 LL).

563

564 Individually, the MAV was involved for less than 100% in the ATE of these four events (Fig. 10 and 11). This contribution
565 fluctuated significantly across the entities from 0% to 100% and according the event. During the 2001 HL, the contribution
566 of the MAV was larger than that of the DV. Conversely during the 1992 LL, the respective contribution of the MAV and DV
567 was rather similar.

568

569 Compared to type iD, iMD and cAM entities, differences between the contribution of the LFV in ATE during HL and LL
570 events are less striking (Fig. 10 and 11). In addition, due to the quasi-equal energy distribution between MAV and DV (even
571 if they remain rather weak in total variability), the severity of LL and HL is dependent on the amplitude of both MAV and
572 DV (Fig. 12a; Grandes-Loges). The MAV primarily guided the emergence of a HL or a LL, while the DV accentuated or



573 attenuated these HL or LL. In addition, the predominant AV can even more accentuate or attenuate the HL severity but also
574 that of LL.

575 **7. Discussion**

576 The present study showed the large influence of the MAV on groundwater LL occurrence in types iMD, cAM, cA aquifers.
577 Simultaneously, the DV modulates the severity of droughts in aquifers for which it accounts for a significant part of GWL
578 variability (types iMD or cA aquifers). Therefore in such contexts, the DV can significantly mitigate LL or amplify LL
579 amplitude. When the DV only accounts for a small part of total variability, then the severity of droughts mainly depends on
580 the amplitude of MAV. These observations are also valid for groundwater HL, but the influence (in proportion) of LFV on
581 HL is mitigated compared to LL since the amplitude of high-frequency variabilities (infra-annual to annual variabilities)
582 strengthen during wet periods (Fig. 12).

583

584 These LFVs, modulated in variance by catchments properties, are directly linked to internal climate variability
585 (Gudmundsson et al., 2011). Numerous studies highlighted the potential link between the LFVs in hydroclimatic variables
586 over the European continent and the LFVs of well-known climatic or oceanic modes such as the North Atlantic Oscillation
587 (NAO) or the Atlantic Multidecadal Oscillation (AMO) also known as the Atlantic Multidecadal Variability (AMV) (Massei
588 et al., 2010; Boé and Habets, 2014; Neves et al., 2019; Liesch and Wunsch, 2019). Such links have even been very well
589 documented and already very extensively studied for the northern France area in several studies dating back the end of the
590 2000s (Massei et al., 2007; Slimani et al., 2009; El Janyani et al., 2012; Fritier et al., 2012; Massei and Fournier, 2012;
591 Massei et al., 2017).

592

593 In the past, regular changes of hydrological variability (i.e., variance) have been observed at each timescale in numerous
594 studies (Fritier et al., 2012; Dieppois et al., 2013 and 2016; Massei et al., 2010 and 2017; Neves et al., 2019). Knowing the
595 dependence of GWE to LFVs, this aperiodic behaviour can heavily influence the HL and LL severity in aquifers displaying
596 inertial or combined GWL variation types. This is why, we found in our study varying contributions of MAV and DV in



597 GWE emergence. Indeed, there are periods where LFVs can exhibit an attenuated variance (e.g., since the end of 2000's for
598 the ~7-yr variability; Fig. 9f) or on the contrary an accentuated variance (e.g., 1990s to 2000s for the ~7-yr variability; Fig.
599 9f). Hence, HL and LL happening during periods with an increased variance of LFV are generally much more severe than
600 those happening during periods with attenuated variance. Therefore, this aperiodic behaviour of LFVs considerably limits
601 the predictability of groundwater droughts, or more largely of GWE.

602

603 The identification of large-scale atmospheric and oceanic states leading to variance modifications in streamflow,
604 precipitation, groundwater time series is still a major issue. Recently, Haslinger et al. (2021) highlighted that the increase of
605 precipitation variability across the Alps at the interannual timescale can be related to a predominant meridional circulation
606 (linked to a positive SST anomaly gradient) enhancing soil moistures feedbacks, while the decrease of variability can be
607 related to a predominant zonal circulation (linked to a negative meridional SST anomaly gradient) suppressing soil moistures
608 feedbacks. In addition, they underlined that the increase variability of precipitation occurs during AMV positive phases at a
609 ~50-yr timescale. Knowing the large impact of LFV amplitude changes on extreme levels, particularly on GWL due to the
610 low-pass filter effect of aquifers, such studies should be developed to identify the drivers of variability changes for predictive
611 purposes of extreme levels.

612

613 Although the potential link between hydrological variability and climate variability is rather well-established, the long-term
614 forecasting of large-scale variabilities (i.e., multiannual, decadal) remains complex owing to their stochastic nature. Indeed,
615 albeit what is seemingly claimed in some studies, none of these variabilities can be considered periodic, and this is also the
616 case of those constituting the NAO spectrum (e.g., Fernandez et al., 2003) as well as the subsequent variabilities observed in
617 hydrology. This issue constrains the robustness of climate projections, in which the internal climate variability is often
618 poorly reproduced and appears as a major source of uncertainty (Qasmi et al., 2017). For instance, Terray and Boé (2013)
619 estimated that uncertainties related to internal variability in precipitation projections over France in the middle of the 21st
620 century may be as large as uncertainties due to climate models. Therefore, such uncertainties in precipitation estimation may
621 also have a huge impact on the future estimation of aquifers recharge and in fine on the predictability of GWL and extremes.



622

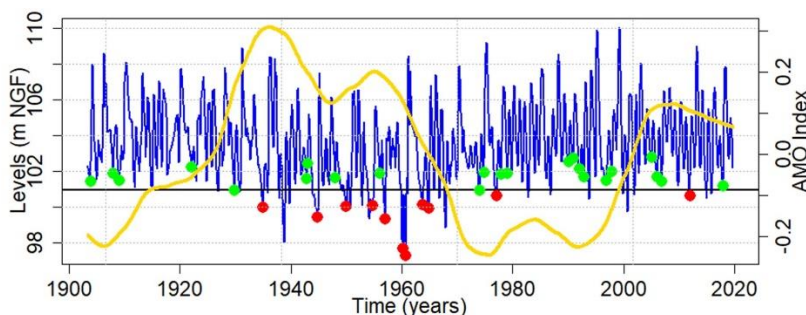
623 It must also be underlined that anthropogenic forcing may have already impacted climate variability (Lenton et al., 2008;
624 Dong et al., 2011; Caesar et al., 2018). Moreover, Feliks et al. (2011) highlighted that interannual variabilities can be
625 suppressed from atmospheric circulation when they are omitted from the Gulfstream front or the SST field. Such
626 modifications of the LFV in large-scale predictors may then influence the hydrological variability. The questions raised by
627 such a phenomenon are: to what extent this could impact the LFV in GWL and then influence extreme levels? Would that
628 lead to more extreme levels or less extreme levels? Would that lead to more or to less severe extremes? Would this be
629 expressed in the same way in aquifers exhibiting different GWL variation types?

630

631 The analysis of a long-term time series shows the importance of historical hindsight, particularly to highlight the influence of
632 a multidecadal variability on GWE. This multidecadal variability displayed by the Tincques time series when filtering MAV
633 and DV is also highlighted in streamflows through metropolitan France (Boé and Habets, 2014; Bonnet et al., 2017 and
634 2020). The links between this variability in streamflow and the AMV have been robustly established by Boé and Habets
635 (2014), Bonnet et al. (2020), and previously in spring precipitation by Sutton and Dong (2012). The negative phase of
636 multidecadal variability in streamflows and precipitation over the 1940-1960 period (corresponding to a warm period of the
637 AMV) is also exhibited in GWL of the Artois-Picardy chalk, hindering the ATE of LL to be fully explained by the MAV and
638 DV (Fig. 14). Low GWL are thus supported by a multidecadal variability seemingly associated to the multidecadal
639 variability in AMV. The short-term analysis could not highlight the significant contribution of multidecadal variability in
640 GWE emergence.

641

642



643

644 **Figure 14: Same as figure 8 but only for the Tincques' GWL filtered of both ~7-yr (MAV) and ~17-yr (DV) components, with the**
645 **Atlantic Multidecadal Variability (AMV) index superimposed in yellow. The AMV is smoothed to highlight the multidecadal**
646 **variability.**

647

648 The historical hindsight available for the Tincques time series also allowed us to observe tougher droughts before the 1960's,
649 certainly related to the negative phase of the multidecadal variability (Fig. 8a). Nonetheless, the most severe drought in the
650 Seno-Turonian chalk of Artois-Picardy appeared around 1921 (during a positive phase of the multidecadal variability). This
651 drought was also identified as one of the most severe events across Europe in precipitation and streamflow time series
652 (Folland et al., 2015; Caillouet et al., 2017; Rudd et al., 2017; Hanel et al., 2018; Barker et al., 2019). Bonnet et al. (2020)
653 also identified this event as the most severe hydrological drought in the Seine river flows. However in their study, this
654 drought did not appear as the most severe in the Beauce limestones (Tourey time series), probably due to the high inertial
655 nature of this hydrogeological entity. Indeed in the chalk (Tincques time series), the 1921 drought seemed to be the result of
656 the combination between a low multi-annual level and a low decadal level (Fig. 9d). The combination of both components
657 explained almost exclusively the drought emergence. In the Beauce limestones, the MAV is poorly expressed in the GWL
658 signal, while the larger scale variabilities (decadal to multidecadal) are widely expressed, therefore the drought of 1921
659 could not have been as severe in the Beauce limestones as it was in the Seno-Turonian chalk, due to the significant role of
660 the MAV in its emergence. Nevertheless, the positive phase of the multidecadal variability probably mitigated the severity of
661 this drought in both aquifers.

662



663 The above example shows that a severe hydrogeological event in a given aquifer, supported by specific low-frequency
664 variabilities, may not be as severe in another aquifer when these variabilities are not or poorly significant in total GWL
665 variability. It highlights the resistance of aquifers to drought events for which the low-frequency components that support
666 them do not constitute a significant part of GWL variability.

667

668 Since these hydrogeological extremes are supported primarily by the LFVs in aquifers with inertial or combined GWL
669 variation types, and considering the large impact that they can induce on our societies (e.g., water exploitation, groundwater-
670 river exchanges, floods), it is necessary to identify the large-scale predictors of such variabilities for extreme levels
671 prediction purposes. In the literature, it has been demonstrated that large-scale patterns leading to the different LFVs (i.e.,
672 multiannual, decadal) may vary across timescales (Massei et al., 2017; Sidibe et al., 2019). Such an approach should be also
673 conducted for GWL. In addition, the response of GWE to scenarios of changing climate variability (i.e., variance changes of
674 LFVs) should also be investigated.

675 **8. Conclusion**

676 This study highlighted the heavy influence of the low-frequency variabilities (LFVs) on the occurrence of high and low
677 groundwater levels (GWL). First, we estimated the proportion of high levels (HL) and low levels (LL) among the total
678 number of their respective occurrences, that were generated by LFVs (typically, multi-annual and decadal variabilities) in
679 Paris Basin aquifers. These proportions were highly dependent on GWL variation types: for aquifers of type iD (inertial –
680 decadal dominant) and iMD (inertial – multi-annual and decadal dominant) occurrences of HL and LL were logically
681 strongly influenced by LFV, conversely to type cA (combined – annual dominant) and cAM (combined – annual and multi-
682 annual dominant) aquifers. In addition, the multidecadal variability also seemed to influence occurrences of HL and LL, but
683 it was only discernable on a 100-yr GWL time series.

684

685 Second, we determined the contribution of the LFVs to the amplitude of threshold exceedance (ATE) during four historical
686 events. Results highlighted that the contribution of the LFV was rather dependent on the significance of multi-annual and



687 decadal variabilities in the total GWL variability. This contribution varied according to the event. Generally, we also
688 observed a more significant contribution of the LFV in the ATE during LL compared to HL. This is related to the higher
689 contribution of high-frequency variability (infra-annual to annual) in HL events, since its variance increases during wet
690 periods, thus reducing the relative contribution of the LFV in the ATE of HL.

691

692 This study also highlighted that the occurrence of a HL or LL and its amplitude (or severity) seemed primarily guided by the
693 multi-annual variability in types iMD, cAM, and cA aquifers. The HL or LL severity can then be significantly accentuated
694 (e.g., 2001 HL, 1992 LL) or attenuated (e.g., 1995 HL, 1998 LL) by the decadal variability.

695

696 This study presented evidence about the key role of LFV in the occurrence of HL and LL. Since LFV originates from large-
697 scale stochastic climate variability as demonstrated in many previous studies in the Paris Basin or nearby regions, our results
698 point out that i) poor representation of LFV in GCM outputs used afterwards for developing hydrological projections can
699 result in strong uncertainty in the assessment of future hydrogeological extremes, ii) potential changes in the amplitude of
700 LFV, be they natural or induced by global climate change, may lead to substantial changes in the occurrence and severity of
701 hydrogeological extremes for the next decades. In addition, such stochastic nature of LFV does not enable any deterministic
702 prediction for future hydrogeological extremes on mid- and long term horizons (i.e., several years or longer). For mid- and
703 long-term hydrogeological extremes prediction purposes, identifying large-scale ocean-atmosphere drivers leading to such
704 variabilities in GWL remains fundamental. Finally, future research should investigate to what extent potential changes in the
705 amplitude of internal climate modes driving LFV could impact hydrogeological extremes.

706 **Data availability**

707 The groundwater level data used for this analysis can be obtained from <https://ades.eaufrance.fr/> (last access: 1st April 2020).
708 For the database of relatively undisturbed GWL time series regarding water abstraction, contact us. The Safran precipitation
709 data set can be obtained from <https://donneespubliques.meteofrance.fr/> (last access: 1st April 2020).



710 **Authors contributions**

711 LB, and NM conceptualized the study. LB took responsibility for the methodology, software, formal analysis, investigation,
712 original draft preparation, and visualization. LB, NM, DA, MF, and HB validated the study. LB collected the resources and
713 curated the data. LB, NM, DA, MF, and HB reviewed and edited the paper.

714 **Competing interests**

715 The authors declare that they have no conflict of interest.

716 **Acknowledgments**

717 This work was partially supported by the GeoERA project TACTIC, funded by the European Union's Horizon 2020 research
718 and innovation programme under grant agreement number 731166. We would also like to thank the Agence de l'Eau Seine
719 Normandie, PIREN Seine, BRGM and Région Normandie for their financial support. Finally, we would like to thank Sandra
720 Lanini for the calculation of effective precipitation.

721 **References**

722 Barker, L. J., Hannaford, J., Parry, S., Smith, K. A., Tanguy, M., and Prudhomme, C.: Historic hydrological droughts 1891–
723 2015: systematic characterisation for a diverse set of catchments across the UK, *Hydrol. Earth Syst. Sci.*, 23, 4583–4602,
724 <https://doi.org/10.5194/hess-23-4583-2019>, 2019.

725

726 Baulon, L., Allier, D., Massei, N., Bessiere, H., Fournier, M., and Bault, V.: Influence de la variabilité basse-fréquence des
727 niveaux piézométriques sur l'occurrence et l'amplitude des extrêmes, *Géologues*, 53–60, 2020.

728

729 Berghuijs, W. R., Woods, R. A., Hutton, C. J., and Sivapalan, M.: Dominant flood generating mechanisms across the United
730 States, *Geophys. Res. Lett.*, 43, 4382–4390, <https://doi.org/10.1002/2016GL068070>, 2016.

731



732 Bertola, M., Viglione, A., Vorogushyn, S., Lun, D., Merz, B., and Blöschl, G.: Do small and large floods have the same
733 drivers of change? A regional attribution analysis in Europe, *Hydrol. Earth Syst. Sci.*, 25, 1347–1364,
734 <https://doi.org/10.5194/hess-25-1347-2021>, 2021.

735

736 Bloomfield, J. P. and Marchant, B. P.: Analysis of groundwater drought building on the standardised precipitation index
737 approach, *Hydrol. Earth Syst. Sci.*, 17, 4769–4787, <https://doi.org/10.5194/hess-17-4769-2013>, 2013.

738

739 Blöschl, G., Hall, J., Viglione, A., Perdigão, R. A. P., Parajka, J., Merz, B., Lun, D., Arheimer, B., Aronica, G. T., Bilibashi,
740 A., Boháč, M., Bonacci, O., Borga, M., Čanjevac, I., Castellarin, A., Chirico, G. B., Claps, P., Frolova, N., Ganora, D.,
741 Gorbachova, L., Gül, A., Hannaford, J., Harrigan, S., Kireeva, M., Kiss, A., Kjeldsen, T. R., Kohnová, S., Koskela, J. J.,
742 Ledvinka, O., Macdonald, N., Mavrova-Guirguinova, M., Mediero, L., Merz, R., Molnar, P., Montanari, A., Murphy, C.,
743 Osuch, M., Ovcharuk, V., Radevski, I., Salinas, J. L., Sauquet, E., Šraj, M., Szolgay, J., Volpi, E., Wilson, D., Zaimi, K., and
744 Živković, N.: Changing climate both increases and decreases European river floods, *Nature*, 573, 108–111,
745 <https://doi.org/10.1038/s41586-019-1495-6>, 2019.

746

747 Boé, J. and Habets, F.: Multi-decadal river flow variations in France, *Hydrol. Earth Syst. Sci.*, 18, 691–708,
748 <https://doi.org/10.5194/hess-18-691-2014>, 2014.

749

750 Bonnet, R., Boé, J., Dayon, G., and Martin, E.: Twentieth-Century Hydrometeorological Reconstructions to Study the
751 Multidecadal Variations of the Water Cycle Over France, *Water Resour. Res.*, 53, 8366–8382,
752 <https://doi.org/10.1002/2017WR020596>, 2017.

753

754 Bonnet, R., Boé, J., and Habets, F.: Influence of multidecadal variability on high and low flows: the case of the Seine basin,
755 *Hydrol. Earth Syst. Sci.*, 24, 1611–1631, <https://doi.org/10.5194/hess-24-1611-2020>, 2020.

756



- 757 Caesar, L., Rahmstorf, S., Robinson, A., Feulner, G., and Saba, V.: Observed fingerprint of a weakening Atlantic Ocean
758 overturning circulation, *Nature*, 556, 191–196, <https://doi.org/10.1038/s41586-018-0006-5>, 2018.
759
- 760 Caillouet, L., Vidal, J.-P., Sauquet, E., Devers, A., and Graff, B.: Ensemble reconstruction of spatio-temporal extreme low-
761 flow events in France since 1871, *Hydrol. Earth Syst. Sci.*, 21, 2923–2951, <https://doi.org/10.5194/hess-21-2923-2017>, 2017.
762
- 763 Constantine, W., and Percival, D.: wmtsa: Wavelet Methods for Time Series Analysis. R package version 2.0-1.
764 <<https://CRAN.R-project.org/package=wmtsa>>, 2016.
765
- 766 Cornish, C. R., Percival, D. B., and Bretherton, C. S.: The WMTSA Wavelet Toolkit for Data Analysis in the Geosciences.
767 *EOS Trans AGU*. 84(46): Fall Meet. Suppl., Abstract NG11A-0173, 2003.
768
- 769 Cornish, C. R., Bretherton, C. S., and Percival, D. B.: Maximal Overlap Wavelet Statistical Analysis With Application to
770 Atmospheric Turbulence, *Bound.-Lay. Meteorol.*, 119, 339–374, <https://doi.org/10.1007/s10546-005-9011-y>, 2006.
771
- 772 Deneux, M., and Martin, P.: Les inondations de la Somme, établir les causes et les responsabilités de ces crues, évaluer les
773 coûts et prévenir les risques d’inondations, Rapport de commission d’enquête (2001–2002), rapport du Senat
774 <<http://www.senat.fr/rap/r01-034-1/r01-034-11.pdf>>, 2001.
775
- 776 Dieppois, B., Durand, A., Fournier, M., and Massei, N.: Links between multidecadal and interdecadal climatic oscillations in
777 the North Atlantic and regional climate variability of northern France and England since the 17th century, *J. Geophys. Res.:*
778 *Atmos.*, 118, 4359–4372, <https://doi.org/10.1002/jgrd.50392>, 2013.
779



780 Dieppois, B., Lawler, D. M., Slonosky, V., Massei, N., Bigot, S., Fournier, M., and Durand, A.: Multidecadal climate
781 variability over northern France during the past 500 years and its relation to large-scale atmospheric circulation, *Int. J.*
782 *Climatol.*, 36, 4679–4696, <https://doi.org/10.1002/joc.4660>, 2016.

783
784 Dong, B., Sutton, R. T., and Woollings, T.: Changes of interannual NAO variability in response to greenhouse gases forcing,
785 *Clim. Dyn.*, 37, 1621–1641, <https://doi.org/10.1007/s00382-010-0936-6>, 2011.

786
787 Edijatno, and Michel, C.: Un modèle pluie-débit journalier à trois paramètres, *La Houille Blanche*, 2, 113–122,
788 <https://doi.org/10.1051/lhb/1989007>, 1989.

789
790 El Janyani, S., Massei, N., Dupont, J.-P., Fournier, M., and Dörfliger, N.: Hydrological responses of the chalk aquifer to the
791 regional climatic signal, *J. Hydrol.*, 464–465, 485–493, <https://doi.org/10.1016/j.jhydrol.2012.07.040>, 2012.

792
793 Fatichi, S., Rimkus, S., Burlando, P., and Bordoy, R.: Does internal climate variability overwhelm climate change signals in
794 streamflow? The upper Po and Rhone basin case studies, *Sci. Total. Environ.*, 493, 1171–1182,
795 <https://doi.org/10.1016/j.scitotenv.2013.12.014>, 2014.

796
797 Feliks, Y., Ghil, M., and Robertson, A. W.: The Atmospheric Circulation over the North Atlantic as Induced by the SST
798 Field, *J. Climate*, 24, 522–542, <https://doi.org/10.1175/2010JCLI3859.1>, 2011.

799
800 Fernández, I., Hernández, C. N., and Pacheco, J. M.: Is the North Atlantic Oscillation just a pink noise?, *Physica A*, 323,
801 705–714, [https://doi.org/10.1016/S0378-4371\(03\)00056-6](https://doi.org/10.1016/S0378-4371(03)00056-6), 2003.

802



803 Flipo, N., Monteil, C., Poulin, M., Fouquet, C. de, and Krimissa, M.: Hybrid fitting of a hydrosystem model: Long-term
804 insight into the Beauce aquifer functioning (France), *Water Resour. Res.*, 48, W05509,
805 <https://doi.org/10.1029/2011WR011092>, 2012.

806

807 Flipo, N., Gallois, N., Labarthe, B., Baratelli, F., Viennot, P., Schuite, J., Rivière, A., Bonnet, R., and Boé, J.: Pluri-annual
808 Water Budget on the Seine Basin: Past, Current and Future Trends, in: *The Seine River Basin*, vol. 90, edited by: Flipo, N.,
809 Labadie, P., and Lestel, L., Springer International Publishing, Cham, 59–89, https://doi.org/10.1007/698_2019_392, 2020.

810

811 Folland, C. K., Hannaford, J., Bloomfield, J. P., Kendon, M., Svensson, C., Marchant, B. P., Prior, J., and Wallace, E.:
812 Multi-annual droughts in the English Lowlands: a review of their characteristics and climate drivers in the winter half-year,
813 *Hydrol. Earth Syst. Sci.*, 19, 2353–2375, <https://doi.org/10.5194/hess-19-2353-2015>, 2015.

814

815 Fritier, N., Massei, N., Laignel, B., Durand, A., Dieppois, B., and Deloffre, J.: Links between NAO fluctuations and inter-
816 annual variability of winter-months precipitation in the Seine River watershed (north-western France), *C. R. Geosci.*, 344,
817 396–405, <https://doi.org/10.1016/j.crte.2012.07.004>, 2012.

818

819 Gouhier, T.C., and Grinsted, A.: biwavelet: Conduct univariate and bivariate wavelet analyses. R package version 0.12.
820 <http://CRAN.R-project.org/package=biwavelet>, 2012.

821

822 Gu, L., Chen, J., Xu, C.-Y., Kim, J.-S., Chen, H., Xia, J., and Zhang, L.: The contribution of internal climate variability to
823 climate change impacts on droughts, *Sci. Total. Environ.*, 684, 229–246, <https://doi.org/10.1016/j.scitotenv.2019.05.345>,
824 2019.

825

826 Gudmundsson, L., Tallaksen, L. M., Stahl, K., and Fleig, A. K.: Low-frequency variability of European runoff, *Hydrol.*
827 *Earth Syst. Sci.*, 15, 2853–2869, <https://doi.org/10.5194/hess-15-2853-2011>, 2011.



828

829 Habets, F., Gascoïn, S., Korkmaz, S., Thiéry, D., Zribi, M., Amraoui, N., Carli, M., Ducharne, A., Leblois, E., Ledoux, E.,
830 Martin, E., Noilhan, J., Ottlé, C., and Viennot, P.: Multi-model comparison of a major flood in the groundwater-fed basin of
831 the Somme River (France), *Hydrol. Earth Syst. Sci.*, 14, 99–117, <https://doi.org/10.5194/hess-14-99-2010>, 2010.

832

833 Hanel, M., Rakovec, O., Markonis, Y., Máca, P., Samaniego, L., Kyselý, J., and Kumar, R.: Revisiting the recent European
834 droughts from a long-term perspective, *Sci. Rep.*, 8, 9499, <https://doi.org/10.1038/s41598-018-27464-4>, 2018.

835

836 Haslinger, K., Hofstätter, M., Schöner, W., and Blöschl, G.: Changing summer precipitation variability in the Alpine region:
837 on the role of scale dependent atmospheric drivers, *Clim. Dyn.*, <https://doi.org/10.1007/s00382-021-05753-5>, 2021.

838

839 Hirabayashi, Y., Mahendran, R., Koirala, S., Konoshima, L., Yamazaki, D., Watanabe, S., Kim, H., and Kanae, S.: Global
840 flood risk under climate change, *Nat. Clim. Change*, 3, 816–821, <https://doi.org/10.1038/nclimate1911>, 2013.

841

842 Hodgkins, G. A., Whitfield, P. H., Burn, D. H., Hannaford, J., Renard, B., Stahl, K., Fleig, A. K., Madsen, H., Mediero, L.,
843 Korhonen, J., Murphy, C., and Wilson, D.: Climate-driven variability in the occurrence of major floods across North
844 America and Europe, *J. Hydrol.*, 552, 704–717, <https://doi.org/10.1016/j.jhydrol.2017.07.027>, 2017.

845

846 IPCC: Managing the Risks of Extreme Events and Disasters to Advance Climate Change Adaptation. A Special Report of
847 Working Groups I and II of the Intergovernmental Panel on Climate Change, Cambridge University Press, Cambridge, United
848 Kingdom and New York, NY, USA, 2012.

849

850 Labat, D.: Recent advances in wavelet analyses: Part 1. A review of concepts, *J. Hydrol.*, 314, 275–288,
851 <https://doi.org/10.1016/j.jhydrol.2005.04.003>, 2005.

852



- 853 Lenton, T. M., Held, H., Kriegler, E., Hall, J. W., Lucht, W., Rahmstorf, S., and Schellnhuber, H. J.: Tipping elements in the
854 Earth's climate system, *P. Natl. Acad. Sci. USA*, 105, 1786–1793, <https://doi.org/10.1073/pnas.0705414105>, 2008.
855
- 856 Liesch, T. and Wunsch, A.: Aquifer responses to long-term climatic periodicities, *J. Hydrol.*, 572, 226–242,
857 <https://doi.org/10.1016/j.jhydrol.2019.02.060>, 2019.
858
- 859 Machard de Gramont, H., and Mardhel, V.: Atlas des remontées de nappes en France métropolitaine, BRGM/RP-54414-FR,
860 105pp, <http://infoterre.brgm.fr/rapports/RP-54414-FR.pdf>, 2006.
861
- 862 Mangini, W., Viglione, A., Hall, J., Hundecha, Y., Ceola, S., Montanari, A., Rogger, M., Salinas, J. L., Borzì, I., and
863 Parajka, J.: Detection of trends in magnitude and frequency of flood peaks across Europe, *Hydrolog. Sci. J.*, 63, 493–512,
864 <https://doi.org/10.1080/02626667.2018.1444766>, 2018.
865
- 866 Maréchal, J.-C. and Rouillard, J.: Groundwater in France: Resources, Use and Management Issues, in: Sustainable
867 Groundwater Management, vol. 24, edited by: Rinaudo, J.-D., Holley, C., Barnett, S., and Montginoul, M., Springer
868 International Publishing, Cham, 17–45, https://doi.org/10.1007/978-3-030-32766-8_2, 2020.
869
- 870 Massei, N. and Fournier, M.: Assessing the expression of large-scale climatic fluctuations in the hydrological variability of
871 daily Seine river flow (France) between 1950 and 2008 using Hilbert–Huang Transform, *J. Hydrol.*, 448–449, 119–128,
872 <https://doi.org/10.1016/j.jhydrol.2012.04.052>, 2012.
873
- 874 Massei, N., Durand, A., Deloffre, J., Dupont, J. P., Valdes, D., and Laignel, B.: Investigating possible links between the
875 North Atlantic Oscillation and rainfall variability in northwestern France over the past 35 years, *J. Geophys. Res.: Atmos.*,
876 112, <https://doi.org/10.1029/2005JD007000>, 2007.
877



878 Massei, N., Laignel, B., Deloffre, J., Mesquita, J., Motelay, A., Lafite, R., and Durand, A.: Long-term hydrological changes
879 of the Seine River flow (France) and their relation to the North Atlantic Oscillation over the period 1950–2008, *Int. J.*
880 *Climatol.*, 30, 2146–2154, <https://doi.org/10.1002/joc.2022>, 2010.

881

882 Massei, N., Dieppois, B., Hannah, D. M., Lavers, D. A., Fossa, M., Laignel, B., and Debret, M.: Multi-time-scale
883 hydroclimate dynamics of a regional watershed and links to large-scale atmospheric circulation: Application to the Seine
884 river catchment, France, *J. Hydrol.*, 546, 262–275, <https://doi.org/10.1016/j.jhydrol.2017.01.008>, 2017.

885

886 McKee, T. B., Doesken, N. J., and Kleist, J.: THE RELATIONSHIP OF DROUGHT FREQUENCY AND DURATION TO
887 TIME SCALES, Eighth Conference on Applied Climatology, Anaheim, California, 17–22, 1993.

888

889 Mishra, A. K. and Singh, V. P.: A review of drought concepts, *J. Hydrol.*, 391, 202–216,
890 <https://doi.org/10.1016/j.jhydrol.2010.07.012>, 2010.

891

892 Neves, M. C., Jerez, S., and Trigo, R. M.: The response of piezometric levels in Portugal to NAO, EA, and SCAND climate
893 patterns, *J. Hydrol.*, 568, 1105–1117, <https://doi.org/10.1016/j.jhydrol.2018.11.054>, 2019.

894

895 Percival, D. B. and Mofjeld, H. O.: Analysis of Subtidal Coastal Sea Level Fluctuations Using Wavelets, *J. Am. Stat. Assoc.*,
896 92, 868–880, <https://doi.org/10.1080/01621459.1997.10474042>, 1997.

897

898 Percival, D. B., and Walden, A. T.: *Wavelet Methods for Time Series Analysis*. Cambridge University Press, Cambridge,
899 2000.

900



901 Pérez Ciria, T., Labat, D., and Chiogna, G.: Detection and interpretation of recent and historical streamflow alterations
902 caused by river damming and hydropower production in the Adige and Inn river basins using continuous, discrete and
903 multiresolution wavelet analysis, *J. Hydrol.*, 578, 124021, <https://doi.org/10.1016/j.jhydrol.2019.124021>, 2019.

904

905 Pointet, T., Amraoui, N., Golaz, C., Mardhel, V., Negrel, P., Pennequin, D., and Pinault, J.-L.: La contribution des eaux
906 souterraines aux crues exceptionnelles de la Somme en 2001 Observations, hypothèses, modélisation, *La Houille Blanche*,
907 89, 112–122, <https://doi.org/10.1051/lhb/2003120>, 2003.

908

909 Qasmi, S., Cassou, C., and Boé, J.: Teleconnection Between Atlantic Multidecadal Variability and European Temperature:
910 Diversity and Evaluation of the Coupled Model Intercomparison Project Phase 5 Models, *Geophys. Res. Lett.*, 44, 11,140-
911 11,149, <https://doi.org/10.1002/2017GL074886>, 2017.

912

913 Rudd, A. C., Bell, V. A., and Kay, A. L.: National-scale analysis of simulated hydrological droughts (1891–2015), *J.*
914 *Hydrol.*, 550, 368–385, <https://doi.org/10.1016/j.jhydrol.2017.05.018>, 2017.

915

916 Rust, W., Holman, I., Corstanje, R., Bloomfield, J., and Cuthbert, M.: A conceptual model for climatic teleconnection signal
917 control on groundwater variability in Europe, *Earth-Sci. Rev.*, 177, 164–174, <https://doi.org/10.1016/j.earscirev.2017.09.017>,
918 2018.

919

920 Rust, W., Holman, I., Bloomfield, J., Cuthbert, M., and Corstanje, R.: Understanding the potential of climate teleconnections
921 to project future groundwater drought, *Hydrol. Earth Syst. Sci.*, 23, 3233-3245, <https://doi.org/10.5194/hess-23-3233-2019>,
922 2019.

923



924 Seguin, J.-J., Allier, D., and Manceau, J.-C.: Contribution d'un index piézométrique standardisé à l'analyse de l'impact des
925 sécheresses sur les ressources en eau souterraine, *Géologues*, 202, 43-48, [https://hal.archives-ouvertes.fr/hal-](https://hal.archives-ouvertes.fr/hal-03219172/document)
926 03219172/document, 2019.

927

928 Sidibe, M., Dieppois, B., Eden, J., Mahé, G., Paturol, J.-E., Amoussou, E., Anifowose, B., and Lawler, D.: Interannual to
929 Multi-decadal streamflow variability in West and Central Africa: Interactions with catchment properties and large-scale
930 climate variability, *Global Planet. Change*, 177, 141–156, <https://doi.org/10.1016/j.gloplacha.2019.04.003>, 2019.

931

932 Slimani, S., Massei, N., Mesquita, J., Valdés, D., Fournier, M., Laignel, B., and Dupont, J.-P.: Combined climatic and
933 geological forcings on the spatio-temporal variability of piezometric levels in the chalk aquifer of Upper Normandy (France)
934 at pluridecennial scale, *Hydrogeol. J.*, 17, 1823, <https://doi.org/10.1007/s10040-009-0488-1>, 2009.

935

936 Sutton, R. T. and Dong, B.: Atlantic Ocean influence on a shift in European climate in the 1990s, *Nat. Geosci.*, 5, 788–792,
937 <https://doi.org/10.1038/ngeo1595>, 2012.

938

939 Terray, L. and Boé, J.: Quantifying 21st-century France climate change and related uncertainties, *C. R. Geosci.*, 345, 136–
940 149, <https://doi.org/10.1016/j.crte.2013.02.003>, 2013.

941

942 Torrence, C. and Compo, G. P.: A Practical Guide to Wavelet Analysis, *B. Am. Meteorol. Soc.*, 79, 61–78,
943 [https://doi.org/10.1175/1520-0477\(1998\)079<0061:APGTWA>2.0.CO;2](https://doi.org/10.1175/1520-0477(1998)079<0061:APGTWA>2.0.CO;2), 1998.

944

945 Trambly, Y., Villarini, G., and Zhang, W.: Observed changes in flood hazard in Africa, *Environ. Res. Lett.*, 15, 1040b5,
946 <https://doi.org/10.1088/1748-9326/abb90b>, 2020.

947



- 948 Van Lanen, H. A. J. and Peters, E.: Definition, Effects and Assessment of Groundwater Droughts, in: Drought and Drought
949 Mitigation in Europe, vol. 14, edited by: Vogt, J. V. and Somma, F., Springer Netherlands, Dordrecht, 49–61,
950 https://doi.org/10.1007/978-94-015-9472-1_4, 2000.
- 951
- 952 Van Loon, A. F.: Hydrological drought explained, *WIREs Water*, 2, 359–392, <https://doi.org/10.1002/wat2.1085>, 2015.
- 953
- 954 Velasco, E. M., Gurdak, J. J., Dickinson, J. E., Ferré, T. P. A., and Corona, C. R.: Interannual to multidecadal climate
955 forcings on groundwater resources of the U.S. West Coast, *J. Hydrol.: Regional Studies*, 11, 250–265,
956 <https://doi.org/10.1016/j.ejrh.2015.11.018>, 2017.
- 957
- 958 Vicente-Serrano, S. M., Beguería, S., and López-Moreno, J. I.: A Multiscalar Drought Index Sensitive to Global Warming:
959 The Standardized Precipitation Evapotranspiration Index, *J. Climate*, 23, 1696–1718,
960 <https://doi.org/10.1175/2009JCLI2909.1>, 2010.
- 961
- 962 Vicente-Serrano, S. M., López-Moreno, J. I., Beguería, S., Lorenzo-Lacruz, J., Azorin-Molina, C., and Morán-Tejeda, E.:
963 Accurate Computation of a Streamflow Drought Index, *J. Hydrol. Eng.*, 17, 318–332,
964 [https://doi.org/10.1061/\(ASCE\)HE.1943-5584.0000433](https://doi.org/10.1061/(ASCE)HE.1943-5584.0000433), 2012.
- 965
- 966 Vicente-Serrano, S. M., Domínguez-Castro, F., Murphy, C., Hannaford, J., Reig, F., Peña-Angulo, D., Trambly, Y., Trigo,
967 R. M., Donald, N. M., Luna, M. Y., Carthy, M. M., Schrier, G. V. der, Turco, M., Camuffo, D., Noguera, I., García-Herrera,
968 R., Becherini, F., Valle, A. D., Tomas-Burguera, M., and Kenawy, A. E.: Long-term variability and trends in meteorological
969 droughts in Western Europe (1851–2018), *Int. J. Climatol.*, 41, E690–E717, <https://doi.org/10.1002/joc.6719>, 2021.
- 970
- 971 Vidal, J.-P., Martin, E., Franchistéguy, L., Baillon, M., and Soubeyroux, J.-M.: A 50-year high-resolution atmospheric
972 reanalysis over France with the Safran system, *Int. J. Climatol.*, 30, 1627–1644, <https://doi.org/10.1002/joc.2003>, 2010.



- 973 Wasko, C. and Nathan, R.: Influence of changes in rainfall and soil moisture on trends in flooding, *J. Hydrol.*, 575, 432–441,
974 <https://doi.org/10.1016/j.jhydrol.2019.05.054>, 2019.